Magdalena Pauritsch, BSc

Use of Polymer Phase Separation During Hot Melt Extrusion to Create Extended Drug Release

MASTER'S THESIS

to achieve the university degree of

Diplom-Ingenieurin

Master's degree programme:

Verfahrenstechnik

submitted to

Graz University of Technology

Supervisors

Univ.-Prof. Dipl.-Ing. Dr.techn. Johannes Khinast
Institute of Process and Particle Technology
Graz University of Technology, Austria

Univ.-Prof. Anette Larsson, PhD
Department of Chemistry and Chemical Engineering
Chalmers University of Technology Gothenburg, Sweden

Gothenburg, June 2021

AFFIDAVIT

I declare that I have authored this thesis independently, that I have not used other than the declared sources/resources, and that I have explicitly indicated all material which has been quoted either literally or by content from the sources used. The text document uploaded to TUGRAZonline is identical to the present master's thesis and has not been submitted before.

Date, Signature

ABSTRACT

Recent findings in pharmaceutical engineering illustrate the necessity to meet new structural demands, as well as the aspiration to accomplish an expansion of personalized medicine. This thesis shows a novel way to address these goals by utilizing the phase separation of a blend containing a hydrophilic and a hydrophobic polymer in hot-melt extrusion (HME). The phase separation is used as an advantage to design extended drug release profiles. To characterise the extruded filaments with different polymer ratios and drug contents, several quantitative and qualitative analysis methods were used, e.g. DSC, WAXS, FTIR-Spectroscopy, SEM and dissolution studies. The results show that the polymers phase separate during HME, and the drug is embedded in both phases. The formation of amorphous solid dispersions, to increase the water solubility of the drug, is successful for all investigated formulations. Furthermore, there seems to be limited interaction between the drug and the polymers and no strong interaction between the two polymers. Release studies demonstrate the possibility to obtain various drug release profiles, with significantly different release rates, by simply adjusting the ratio of the hydrophilic and the hydrophobic polymer or the drug content. Overall, this work demonstrates that no compromise is necessary, by selecting either a hydrophobic or a hydrophilic polymer in formulation development, depending on the desired properties. A polymer blend and the utilization of the phase separation provide a promising approach without the costly and complex necessity to approve new substances.

KURZFASSUNG

Jüngste Forschungsergebnisse im Bereich der Pharmazietechnik illustrieren die Notwendigkeit, neuen strukturellen Anforderungen gerecht zu werden, sowie das Bestreben das Konzept von personalisierter Medizin auszudehnen. Diese Arbeit demonstriert eine neue Möglichkeit diese Ziele zu erreichen, indem die Phasentrennung einer Mischung aus einem hydrophilen und einem hydrophoben Polymer, während dem Extrudieren, genutzt wird. Diese Phasentrennung kann als Vorteil in Bezug auf das Design von verlängerten Freisetzungsprofilen gesehen werden. Um die extrudierten Filamente zu charakterisieren, werden verschiedene quantitative und qualitative Analysemethoden, z.B. DSC, WAXS, FTIR-Spektroskopie, SEM und Freisetzungstests, durchgeführt. Die Ergebnisse zeigen, dass während dem Extrudieren eine Phasentrennung zwischen den Polymeren stattfindet und der Wirkstoff in beiden Phasen vorliegt. Die Erzeugung von amorphen Feststoffdispersionen, um die Wasserlöslichkeit zu erhöhen, ist für alle getesteten Zusammensetzungen möglich. Außerdem liegen keine starken Anziehungskräfte zwischen dem Wirkstoff und den Polymeren, sowie zwischen den Polymeren selbst vor. Die Freisetzungstests zeigen, dass es nur durch das Verändern des Verhältnisses von hydrophilem zu hydrophobem Polymer oder des Wirkstoffanteils möglich ist, verschiedene Freisetzungsprofile mit deutlich unterschiedlichen Raten zu generieren. Insgesamt zeigt diese Arbeit, dass es nicht notwendig ist in der Entwicklung von Rezepturen mit unterschiedlichen Eigenschaften einen Kompromiss einzugehen, indem man entweder ein hydrophiles oder ein hydrophobes Polymer auswählt. Eine Polymermischung zu verwenden und sich die Phasentrennung zunutze zu machen, stellt damit eine vielversprechende Alternative zur teuren und komplexen Genehmigung neuer Substanzen dar.

ACKNOWLEDGEMENTS

First of all, I would like to thank my supervisors at Chalmers University in Gothenburg, Professor Anette Larsson and Robin Nilsson. Anette helped me with all my questions and supported me in my working progress, however also encouraged me to use my time here in Sweden and explore the country. I really enjoyed our weekly virtual meetings. Many thanks to Robin, who helped me with the different experiments in the lab, explained all the rules and devices to me and made sure I never got lost in the eight-story chemistry building. Additionally, thanks to the researchers at Chalmers who helped me with my experiments, Martina Olsson, Anders Mårtensson, Katarina Logg, Ezio Zanghellini and Matthew Sadd. Thanks to my supervisor at TU Graz, Professor Johannes Khinast, who made it possible in the first place, to work abroad in Sweden on my master's thesis.

A huge thank you to my whole family, especially my mum and dad, for their love, for always believing in me and even supporting the decision to write my master's thesis in Sweden, although it was tough to let me go for quite a long time. Not least to my sister Juliana, for always having my back and giving me perspective on things, when I need it.

Thanks to my best friend Karin, for making me laugh so many times, for always listening to me and never getting tired of reminding me that everything will work out eventually. Additionally, thanks to Juliana and Karin, for proofreading and adding all the commas.

Last but not least, thanks to my girlfriend Leonie, for making our semester abroad so amazing, despite these challenging times. Thank you so much for standing by me, for always supporting me, for your love, encouragement, and patience. I truly could not have done it without you.

LIST OF ABBREVIATIONS

AM	Additive manufacturing
API	Active pharmaceutical ingredient
ASD	Amorphous solid dispersion
ATR-FTIR	Attenuated total reflection – Fourier transformed infrared spectroscopy
BCS	Biopharmaceutical classification system
DSC	Dynamic light scattering
HME	Hot melt extrusion
HPC	Hydroxypropyl cellulose
HPMC	Hydroxypropyl methylcellulose
HSP	Hansen solubility parameters
FDA	Food and drug administration
FDM	Fused deposition modelling
PLA	Polylactic acid
SEM	Scanning electron microscopy
MW	Molecular weight
MEC	Minimum effective concentration
MTC	Minimum toxic concentration
NSAID	Non-steroidal anti-inflammatory drug
NPX	Naproxen
PASD	Polymeric amorphous solid dispersions
Raman	Raman spectroscopy
T_d	Degradation temperature
T_g	Glass transition temperature
T_m	Melting temperature
WAXS	Wide angle X-ray scattering

TABLE OF CONTENT

1 INTRODUCTION

Several novel concepts were investigated in pharmaceutical engineering over the last years. For example the expansion of personalized medicine [1], the utilization of 3D printing technologies [2], [3] or the incorporation of continuous manufacturing alternatives rather than batched based processes[4], [5]. The approach shown in this work has a direct link to each of the just mentioned concepts.

Hot-melt extrusion (HME) is used as a manufacturing method, which is a continuous and solvent-free method to produce amorphous solid dispersions (ASDs) for low water-soluble drugs [6], [7]. Low solubility and bioavailability are frequent issues with novel drug candidates found by high throughput screening and therefore must be addressed to ensure a possible approvement as an active pharmaceutical ingredient (API) in pharmaceutical products [8]. Furthermore, the produced filaments can be used as a starting material in 3D printing [9], [10] and can therefore be considered as a possible manufacturing step in the development of personalized medicine [10].

The objective of this thesis, however, is not to use a single polymer to form an ASD but a polymer blend of a hydrophilic and a hydrophobic polymer. The use of a polymer blend provides the possibility to use synergistic effects to influence desired properties of the formulations, such as pH independence, tailoring of the release profiles [11], [12] or influencing the crystallisation of a drug [13]. However, it is known that blends of macromolecules tend to phase separate upon mixing [14]. Nonetheless, this polymer phase separation can be seen as an advantage rather than a disadvantage and even be utilized to influence mass transport through films, as shown in a recent work by Andersson [15]. Furthermore, using polymer blends to meet new structural demands avoids the approval of new excipients [11], [12] and the usual trade-off between choosing stability with a hydrophobic or fast release with a hydrophilic polymer [16] can be avoided and potentially utilized to tailor the release profiles.

This thesis aims to investigate the phase separation after HME as a novel way to create extended drug release profiles. The used materials are the hydrophilic and semisynthetic cellulose derivative hydroxypropyl methylcellulose (HPMC) and the hydrophobic, thermoplastic and biocompatible polymer polylactic acid (PLA). As a model drug, the non-steroidal anti-inflammatory drug (NSAID) Naproxen, is used.

The filaments are manufactured with a rotating twin screw extruder and characterised quantitatively and qualitatively by several analysis methods because the complex morphology and properties of ASDs cannot be determined with only one analysis method [17], [18].

In the first two chapters of this thesis the underlying theoretical phenomena relevant for this work are discussed and the used materials and methods are described. The subsequent chapters detail the obtained results. First, the miscibility of the compounds is theoretically estimated with the Hansen Solubility Parameters, subsequently different mixtures are extruded and analysed with DSC, WAXS and ATR-FTIR spectroscopy to determine physical properties or chemical modifications and get insight into the phase behaviour. Additionally, prior to the in vitro studies, Raman mapping is performed, to characterise the phase separation after extrusion. Furthermore, dissolution studies are carried out, to test the influence of different polymer ratios and drug contents on the release behaviour of the drug. Afterwards, SEM is utilized to analyse the remaining polymer matrix after release.

2 THEORETICAL BACKGROUND

The most critical theoretical phenomena that are relevant for this project are described in this chapter. First, the principles of personalized medicine and hot-melt extrusion (HME) are introduced. Second, the use of polymers in the pharmaceutical industry and polymer phase separation, as well as the state of the art in the formulation development of solid dispersions are outlined. Furthermore, general drug release mechanisms from polymeric carriers and extended drug release are discussed.

2.1 PERSONALIZED MEDICINE

Personalized medicine has gained a lot of interest in pharmaceutical research and is considered the next major step towards an improvement of health outcomes [1]. The concept of personalized medicine is characterised by patient specific tailoring of drug dose and formulation to meet the specific needs of an individual patient [1], [10]. The approach evolved from the observations of varying responses of individual persons to the same formulation or dosage form. Although these observations date back to the late 1950's [10], the pharmaceutical industry is still dominated by the concept of "one fits all" and has therefore directed the industry to mass production [1]. Govender et al., proposed the new and innovative concept of mass customization realised via a modularized product design concept [19]. While this concept would revolutionize personalized medicine, specific manufacturing technologies are needed to ensure affordable and high-quality products for a holistic treatment of individual patients [10], [19].

One of the most investigated methods to ensure an individual and flexible design approach, needed for realizing a mass customization process in the pharmaceutical industry, are so-called additive manufacturing (AM) methods like 3D printing [2], [10]. With AM methods, the design of a product is not limited to classical geometrical shapes or sizes compared to traditional pharmaceutical formulations. For example, it is possible to provide individual medicine with different release profiles based on the geometric shape of the tablet, since that directly correlates to the drug's release characteristics [2].

In addition, the drug content can also be adjusted easily, based on specific patient needs. One of the most popular AM, due to its affordability, highly flexible equipment and the possibility to use pharmaceutical polymers, is fused deposition modelling (FDM). Additionally, the starting material can be produced by HME, which therefore results in a continuous manufacturing process [20].

By comparing different AM techniques, Govender et al. concluded that FDM is a suitable manufacturing method for the modular concept of individualized medicine [1], [10], [19]. Naturally, there are also shortcomings of this technology, for example, the limitation to thermoplastic materials and thermally

stable APIs and the difficulty of scale-up [1], [21]. The large potential of this technology is indicated by papers on 3D printing currently being published every day, showing the potential of this technology and the possibility to overcome these problems [2].

Hsiao et al. already concluded in a review of 3D printing of oral formulations valid applications in three fields: preclinical drug supply with flexible doses, innovative drug delivery concepts with multiple APIs and varying delivery rates, and decentralized drug manufacturing [21].

The filaments needed for FDM should be in a uniform shape with suitable stability and flexibility [20], [22]. A common method to ensure these properties for the starting material in the FDM printing process is the use of filaments produced by HME [10], [20]. Therefore, HME can be viewed as a promising manufacturing method regarding personalized medicine [22]. Hence this method is further investigated in this study and discussed in the following chapter.

2.2 HOT MELT EXTRUSION

The processing of materials at elevated temperatures and pressure with continuous feeding through a barrel into a product of uniform shape and density is called extrusion. HME therefore involves the compaction and conversion of powder or granulate mixtures into a melt and uniform solid product [23].

The process of HME was first introduced in the 19th century and is currently widely used within the plastic industry [23]–[25]. In the last few decades, it has also been emerging as a manufacturing technique for tablets, pellets and granulates within the pharmaceutical industry [6], [23]. This development is caused, as indicated by multiple publications, by the possibility to enhance the solubility of poorly soluble APIs and consequently also increase the bioavailability, as well as the fact that it is a continuous manufacturing process [6], [7], [23]. The latter might also be a reason for the growing interest in HME, because there is a trend in pharmaceutical manufacturing to investigate the implementation of continuous processes. Continuous processes are known to reduce costs, to be more sustainable and to be easier to manage in terms of safety and process control [4], [5], [26].

The implementation of HME into a manufacturing process can additionally save several process steps, since it includes mixing, granulation and drying in one step [26]. Although almost all pharmaceutical companies are interested in the development and utilization of continuous processes in primary, as well as secondary manufacturing [4], there are still many challenges. One of these being the unwillingness of companies to invest in the development of these processes on an industrial level, while already well-established batch-based alternatives are available on the market [4].

Another shortcoming of the HME process is the limitation to materials with good thermomechanical and flow properties. However, the possibility to process low solubility drugs and the possibility of using novel chemical compounds presents a significant additional advantage of HME as a continuous manufacturing process [4].

The knowledge about large quantities of possible novel drugs results from new methodologies like high-throughput screening [27], which include the screening of large chemical databases for activity against biological targets via automatization, miniaturization and large-scale data analysis [28]. These screenings have already generated large numbers of novel API possibilities, which are poorly soluble and classified in the Biopharmaceutical Classification System (BCS) as class II or IV. This classification generally includes a low bioavailability, and therefore the substances might not be considered as potential novel API. The majority of newly approved drugs in the 20th century are class I substances [29], [30]. With HME however, it is possible to increase the solubility and bioavailability of other substances by creating so-called solid dispersions (cf. chapter 2.4), which leads to a consideration as a viable option in patient treatment [6], [18], [22], [24]. Furthermore, HME is the only solvent-free method to create solid dispersion, which provides another environmental benefit [18].

A schematic HME process can be seen in *Figure 2-1.* In this case, a polymer and an API are fed into a barrel of a rotating twin screw extruder and processed at elevated temperatures.

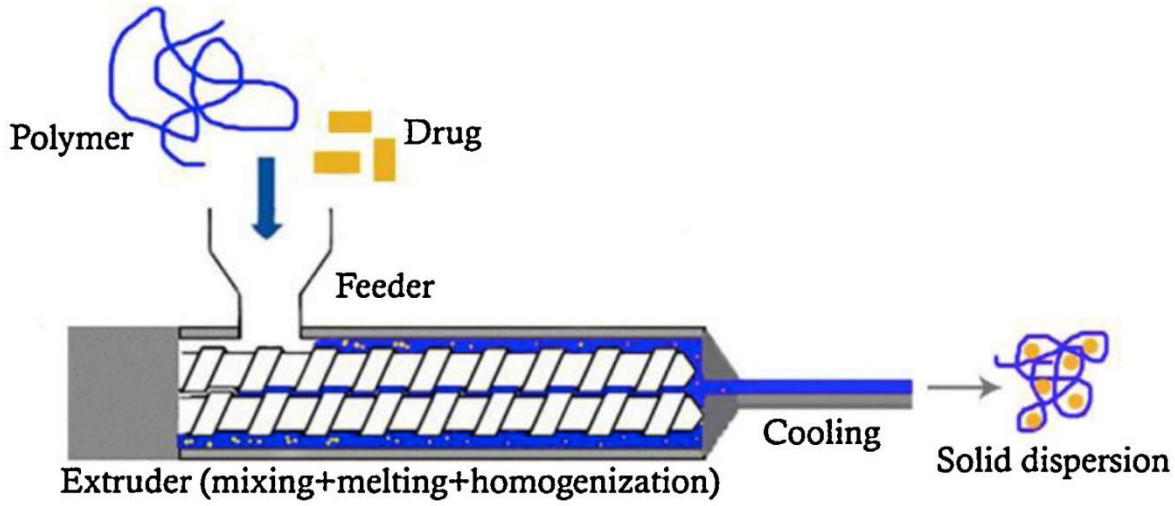

Figure 2-1: HME Process Scheme [25]

The compounds are mixed and homogenized inside the barrel, and subsequently the material is extruded through a die and cools down at room temperature. The created solid dispersion filaments can then be used for further downstream processing like FDM [9], [10], [31].

2.3 POLYMERS IN PHARMACEUTICAL ENGINEERING

A variety of polymers is already widely used in the pharmaceutical industry to provide controlled drug delivery or increase drug stability. Applications include, but are not limited to, tablets, capsules and gels [11]. This section gives an overview of general properties relevant for this work and how to characterise them, as well as provides information about polymer blends and the occurrence of polymer phase separation.

2.3.1 States of Order in Polymers

Polymers can appear in several conformations and configurations of their individual macromolecules. These arrangements, aside from chemical composition or chain length, are crucial for the properties of polymers. Macromolecules can appear in solution, molten-state, solid-state or as liquid-crystalline polymers. Since only the solid-state is relevant for this work, it will be the focus of the remaining chapter. Macromolecules in the solid-state can exist in amorphous or crystalline form, depending on the arrangement of the polymer chains. While a crystalline structure is characterised by ordered regions with regularly arranged chains, the amorphous state displays an irregular non-ordered structure. However, these states are not exclusive to each other and some polymers are in a so-called semicrystalline state with crystalline as well as amorphous regions. The respective thermal phase behaviour of these macromolecules, regardless of the state of order, differs significantly for compounds with low molecular weight (MW) [14].

2.3.2 Thermal Characterisation of Polymers in Bulk

In contrast to low MW compounds, even highly crystalline polymers do not display a sharp melt peak but rather a gradual melting over a wider temperature range. Amorphous polymers, however, do not melt but soften over a broad temperature range and the characteristic quantity describing this softening is called glass transition temperature T_g [14]. Differential scanning calorimetry (DSC) is a common procedure for the thermal characterisation of polymers, and a schematic thermogram of a semicrystalline polymer is displayed in *Figure 2-2*.

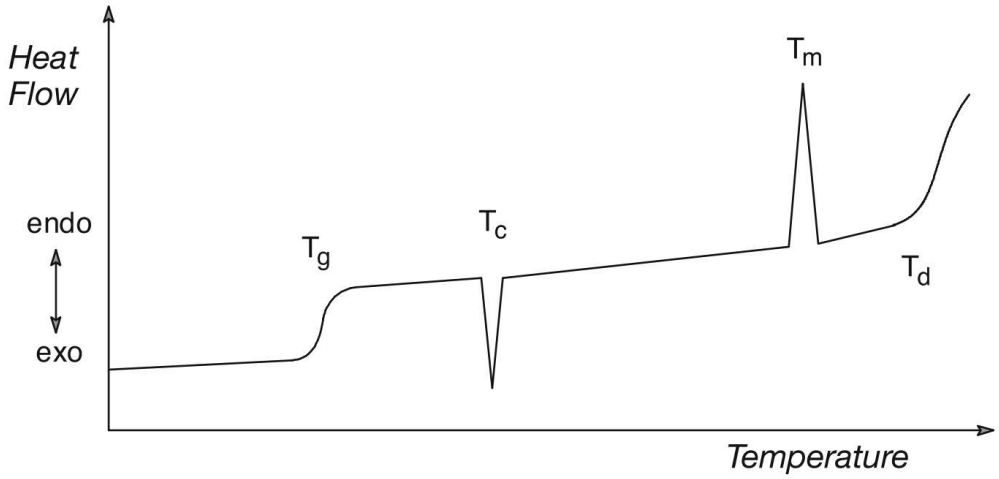

Figure 2-2: Schematic thermogram of a semicrystalline polymer [14]

The thermogram displays characteristic thermal properties of semicrystalline polymers, namely glass transition T_g, crystallisation T_c, melt T_m and degradation T_d temperature. Amorphous polymers, however, do not show a melt or crystallisation peak but only the glass transition and degradation temperature [14].

2.3.3 Polymers and Polymer Blends

Mixtures of two or more different polymers generally are called polymer blends [14]. Blending two polymers and preserving their individual properties as well as using the synergistic effects of the mixture provides an inexpensive and advantageous method to obtain new structural materials [12]. Therefore, these polymer blends can provide significant advantages for the pharmaceutical industry. As mentioned before, pure polymers are already widely used in pharmaceutical products, however, novel drug developments demand new and improved materials to meet the desired requirements. Thus, a blend of already approved and well-known polymers provides an attractive alternative in formulation development, considering the time and resources required for the regulatory approval of new substances [11], [12].

Studies indicate that a polymer mixture can significantly improve desired properties, such as pH-independency or tailored release profiles, due to synergistic effects between the mixed polymers [11], [12]. For example, Van Ngo et al. already demonstrated a promising approach of a hydrophobic-hydrophilic polymer blend for the modulation of crystalline changes and molecular interactions in solid dispersions [13].

2.3.4 Polymer Phase Separation

Although mixing of macromolecules is generally possible in the same way as for other raw materials (e.g. metals), polymers tend to phase separate upon mixing. This behaviour can be explained thermodynamically and is defined by the change in free energy ΔG_{mix} upon mixing, which is defined as stated in *Equation 2-1*, by the entropy ΔS_{mix} and enthalpy ΔH_{mix} of mixing [14].

$$\Delta G_{\mathrm{mix}} = \Delta H_{\mathrm{mix}} - \mathrm{T} \cdot \Delta S_{\mathrm{mix}} \qquad 2\text{-}1$$

A single-phase system is obtained for negative values of ΔG_{mix}, whereas a two-phase system, i.e. a phase separated system, is characterized by a positive value for the change in free energy. By blending two polymers, the condition of a negative ΔG_{mix} is fulfilled far less frequently than for low MW compounds, which can be attributed to very low values of ΔS_{mix}. Although the disorder is increasing for polymers upon mixing too, the values are much lower, due to the higher MW and consequently fewer molecules per volume element. Furthermore, small values for the enthalpy of mixing are also unlikely for polymers because it would require chemically very similar macromolecules [14].

The free energy ΔG_{mix} can be predicted quite well with the Flory-Huggins lattice model [14], [15], however the model fails if crystallisation or strong molecular interactions occur [14]. Aside from thermodynamic calculations with the Flory-Huggins model, a simple way to indicate a phase separation between two polymers is the investigation of the glass transition temperature of the mixture [14], [32], [33].

However, phase separation is not necessarily an undesired phenomenon and could be used as a significant advantage in pharmaceutical engineering. A recent study on films, made of hydrophobic ethyl cellulose and hydrophilic hydroxypropyl cellulose (HPC), which tend to phase separate during spray coating, indicates that this phase separation can be a decisive factor for the development of new formulations and can be used as a way to influence the mass transport through a film. The matrix-forming between the two polymers displays distinct domains of the respective polymers. Therefore, the HPC-rich phase can serve as a template for the pores and consequently influence the release of the drug, for example, in spray-coated pellets [15].

Nevertheless, the determination of the phase behaviour and structural arrangement within a polymer blend is not trivial, and there are several factors influencing the morphology such as, but not limited to, phase volumes, kinetic of segregation, shape of two-phase area, and surface energy [15]. The phase morphology, for example accomplished by HME, significantly influences the physical properties of the

mixtures. However, a certain interfacial bonding between the phases, i.e. a partial compatibility between the matrix and the dispersed phase, is necessary to prohibit a separation of the two phases on macroscale after extrusion [14].

A simple way to determine if two polymers are fully miscible is the determination of the glass transition temperature of the mixture. A miscible polymer blend displays only one T_g, whereas a phase separated system displays two T_gs [14], [32]. Knowledge about the glass transition as a function of composition is therefore decisive for other properties of polymer-based systems [32]. The glass transition can be experimentally determined with DSC or calculated with empirical equations.

The glass transition temperature of a miscible but non-interactive system, except for cohesive and adhesive interactions, can be estimated using equations following simple mixing rules. One example is the Gordon-Taylor equation with an implementation of the Simha-Boyler rule. Gordon and Taylor have shown that ideal co-polymer blends display linearity, reflecting volume additivity, of the components [33]. The equation for the $T_{g,m}$ of mixtures is depicted in *Equation 2-2*, with w_i and δ_i being the weight fraction and density of the components, respectively and k_{ij} is the Gordon-Taylor constant calculated with the Simah-Boyler rule. Terms containing the subscript 3 are excluded for binary mixtures.

$$T_{g,m} = \frac{w_1 \cdot T_{g,1} + k_{12} \cdot w_2 \cdot T_{g,2} + k_{23} \cdot w_3 \cdot T_{g,3}}{w_1 \cdot + k_{12} \cdot w_2 + k_{23} \cdot w_3} \qquad 2\text{-}2$$

$$\text{with } k_{12} = \frac{\delta_1 \cdot T_{g,1}}{\delta_2 \cdot T_{g,2}} \text{ and } k_{23} = \frac{\delta_2 \cdot T_{g,2}}{\delta_3 \cdot T_{g,3}}$$

If the glass transition of polymer blends does not follow this equation, this is either an indication for strong interactions between the polymers or a possible phase separated system if the blend displays two glass transition temperatures [14], [32].

2.3.5 Hydroxypropyl methylcellulose (HPMC)

HPMC is a hydrophilic, water-soluble polymer that is used to create stable ASDs. The repeating unit of HPMC, a polymer with a specially designed substitution architecture that improves thermal processability [34], can be seen in *Figure 2-3*.

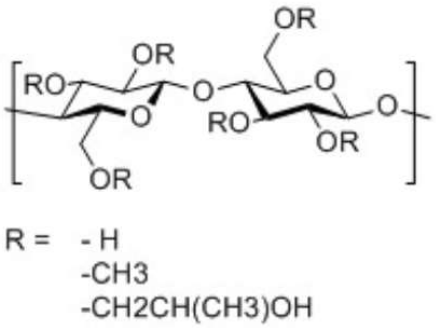

Figure 2-3: Chemical structure of the HPMC polymer: repeating unit [34]

It has a T_g of approximately 115 °*C* and remains stable against thermal degradation up to 250 °*C* [34].

2.3.6 Polylactic Acid (PLA)

Polylactic acid (PLA) is a hydrophobic, aliphatic polyester, cf. chemical structure in *Figure 2-4,* that plays an increasing role in biomedical applications [35]. It is a thermoplastic polymer that has found its entrance into the plastic industry and is partly replacing petrol based polymers, because it has the advantage of being biodegradable, biocompatible and can be produced from renewable feedstock [35], [36].

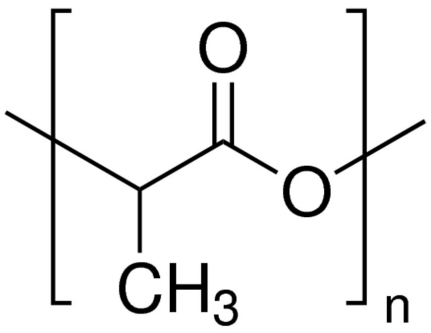

Figure 2-4: Chemical structure of the PLA polymer: repeating unit

In recent years PLA has gained interest for medical applications and was already approved by the US Food-and Drug-Administration (FDA) for human use as bone-implants or formulations of sustained drug delivery [35], [36].

2.4 SOLID DISPERSIONS

Similar to polymers, drug molecules can either exist in a crystalline or an amorphous state. The crystalline form of an API has the advantage of high purity and stability, but the lattice energy barrier is heavily restricting the dissolution. A disordered structure, i.e. an amorphous state, has higher free energy compared to the crystalline form and consequently a higher dissolution rate and therefore a higher

solubility. However, a higher free energy also leads to physical and chemical instability, which is why they are rarely considered in formulation development. However, the advantage of a higher solubility in the amorphous state can be maintained by kinetically stabilizing the API [18].

Currently, the most promising way to achieve this stabilization is the formation of so-called solid dispersions [17], [37]. The label 'solid dispersion' is a broadly used term for a drug dispersed in a carrier matrix. Nonetheless, the drug can exist in various forms within the carrier, depending on composition and processing history, which requests additional specifications [10], [37].

The three possible structures of a solid dispersion between a drug and a polymer are depicted in *Figure 2-5* [10], [37]. The drug can either be molecularly dispersed (A), exist in amorphous form in drug rich domains (B) or precipitate out and recrystallise (C).

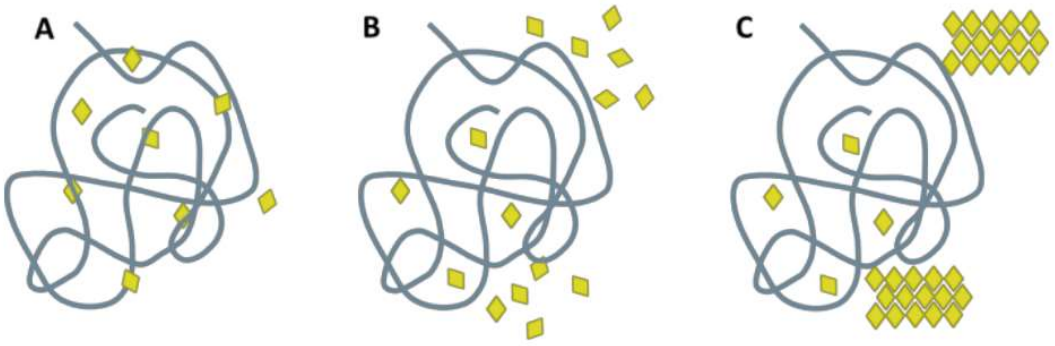

Figure 2-5: Different structures of drug/polymer solid dispersions with a rhombus representing a drug molecule and lines representing polymer chains; (A) drug is molecularly dispersed in the carrier;(B) amorphous drug-rich domains exist; (C) the drug has precipitated out and formed crystalline drug regions [10]

If the drug loading is below the equilibrium solubility a molecular dispersion can be formed, however, that state is only likely at very low drug loadings and high temperatures. Decreasing the temperature leads to a supersaturated solution, and the API shows the tendency to precipitate out. Subsequently that either results in a recrystallisation or the formation of amorphous drug aggregates dispersed in the carrier matrix [37]. Therefore, an increase in solubility and bioavailability can only be achieved by either molecular dispersing the drug or maintaining the drug in an amorphous form and avoiding recrystallisation. The latter desired structure of a solid dispersion is specified as amorphous solid dispersion (ASD) [10], [18].

The two main manufacturing processes to obtain ASDs are solvent evaporation, e.g. spray drying, and melting, e.g. HME. Both processes have different advantages and disadvantages, and the selection of

the process should be based on material characteristics and the desired properties of the final product [29].

2.4.1 Polymeric Amorphous Solid Dispersions (PASD)

To preserve the amorphous state of the drug, polymers can be used as carriers and so-called polymeric amorphous solid dispersions (PASD) are formed [18]. The stability of PASDs is influenced by several factors, such as but not limited to glass transition, molecular mobility, miscibility and preparation method [17], [18]. Polymers are advantageous as carriers because they offer several possibilities to maintain a stable ASD, for example to limit the molecular mobility of the API, due to the structural nature of macromolecules. Crystallisation and phase separation of the drug involve nucleation and diffusion, which require sufficient molecular mobility. The numerous chains and the cross-linked structure of polymers have the possibility to hinder and restrict the mobility of the drug molecules by acting as physical barriers and therefore prohibiting recrystallisation. Furthermore, intermolecular interactions between drug and polymer, such as the formation of hydrogen bonds or anti-plasticization of the drug due to a polymer with a higher T_g, are other possibilities to increase the stability of the drug in the amorphous state [18].

The selection of suitable polymers for the formulation of a PASD with a drug should be based on the characterisation of physiochemical properties of the drug and the polymer. The polymers ideally have a high T_g and a low T_m and furthermore, the polymer should have the same solubility parameters as the drug [18]. This approach is further discussed in *Chapter 2.4.4*.

2.4.2 Naproxen (NPX)

The used model drug Naproxen is a non-steroidal anti-inflammatory drug (NSAID) utilized to treat migraine, rheumatoid arthritis and osteoarthritis. The chemical structure can be seen in *Figure 2-6.*

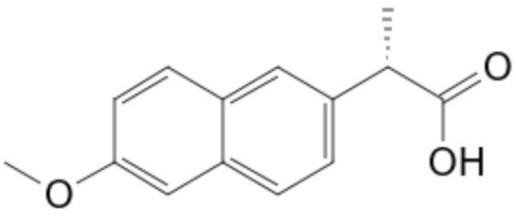

Figure 2-6: Chemical structure of Naproxen

It is considered a poorly water-soluble drug with a relatively low bioavailability leading to challenges in drug manufacturing but also causing severe environmental impact [38], [39].

2.4.3 Characterisation of ASD

Complex physiochemical properties depending on the manufacturing process, and the risk of recrystallisation, require several comprehensive complementary analysis methods. No single characterisation method can give insight into all relevant properties [17]. Quantitative as well as qualitative methods should be used to characterise ASDs. It is not within the scope of this thesis to describe them all, but a brief selection is provided. Analysis methods for the characterisation of ASDs include but are not limited to [17]:

- thermal analysis methods including calorimetric techniques such as differential scanning calorimetry (DSC)
- microscopic and morphological analysis, e.g. powder X-ray diffraction or scanning electron microscopy (SEM)
- spectroscopy techniques (solid-state nuclear magnetic resonance, infrared and Raman spectroscopy)

2.4.4 Hansen Solubility Parameters

A widely used idea to solve complex formulation issues are to use the so-called Hansen Solubility Parameters (HSP; note that the abbreviation is plural) [40]. While the parameters were initially developed by Hansen on the basis of the Hildebrand parameter to predict the solubility of polymers in various solvents, the concept has been further developed and extended to predict solubility and similarity of various materials [40], [41]. However, solubility is not always an accurate description, and frequently the broader terms similarity and compatibility are used [40]. HSP, in contrast to the Hildebrand theory, consist of three parameters δ_D, δ_P, δ_H, related to the three major interaction types in organic materials: non-polar interactions also called dispersion interactions (δ_D), polar dipol-dipol interactions caused by polar cohesive energy (δ_P), as well as hydrogen bonds (δ_H) [40], [41]. With these parameters, polymer compatibility and the solubility of a drug within a polymer can be estimated. Although the method has known drawbacks, it still provides a valuable tool in formulation development due to its balance of accuracy and simplicity [40]. The parameters can either be calculated with group contribution methods such as the Hoy and Van Krevelen method, determined experimentally via solubility measurements in different solvents and calculated with 'sphere-method' or determined with molecular dynamics [42]. In this thesis a simple estimation is made based on the so called 'distance' between two materials [41], [42], depicted in *Equation 2-3*. Furthermore, the HSP can be displayed in a 3D plot and a radius can be

determined depending on, if a compound is soluble (distance = 0) or not soluble (distance = 1) in a solvent. The calculated radius includes all the solvents where the compound is soluble and excludes others. With these 3D plots the similarity or compatibility of two materials can be visualized.

$$distance = \left[4 \cdot \left(\delta_{D,1} - \delta_{D,2}\right) + \left(\delta_{P,1} - \delta_{P,2}\right) + \left(\delta_{H,1} - \delta_{H,2}\right)\right]^{1/2} \qquad 2\text{-}3$$

To determine the similarity of two polymers the overlap of the two spheres is usually calculated, however for that method the radius of the polymers must be known. For a drug and a polymer, a small distance indicates that the materials are sufficiently alike, and therefore the drug will not likely precipitate out of the polymer matrix over time [42].

2.5 DRUG RELEASE BEHAVIOUR

The development of new pharmaceutical products involves several selection steps of APIs, excipients and manufacturing processes. The validation of the obtained products is assessed by determining the in vitro performance and quality attributes as well as executing in vivo studies or modelling in vivo performances to determine effectiveness and safety [43].

The success of developing ASDs can ultimately be determined by the performance of the drug in dissolution [37]. The most used methods are dissolution studies with release media simulating human intestinal fluids. Consequently, the results can be used in *in vitro-in vivo* correlations to estimate the in vivo performance of the formulation [18], [43]. Nonetheless, it can be challenging to develop accurate models because the underlying phenomena for the drug release are quite complex [18].

In principle there are two dissolution regimes that can be observed depending on the drug loading. At lower drug loadings, the release is controlled by the polymer release speed (especially for hydrophilic polymers), and at higher drug loadings, the drug release is determining the release rate [16], [44]. The limit for the change in rate control between drug and polymer, however, is significantly influenced by the used polymers and the drug as demonstrated by Saboo et al. [16]. Concerning the hydrophilicity of the polymer, it is observed that higher drug loadings are achievable with hydrophobic polymers, but faster release rates are possible with hydrophilic polymers [16].

The general solubilization mechanism of PASDs is the so-called spring and parachute concept [18], [37], which will be explained in the following chapter. Furthermore, the concept of controlled drug extended release will be discussed briefly.

2.5.1 Solubilization Mechanism of PASDs

The general concept of solubilization techniques is the "spring and parachute" concept illustrated in *Figure 2-7*. The drug in the crystalline form has a very low solubility, whereas the drug in the amorphous form shows a solubility peak (spring), followed by a sharp decrease due to the metastability of the amorphous state [18], [37].

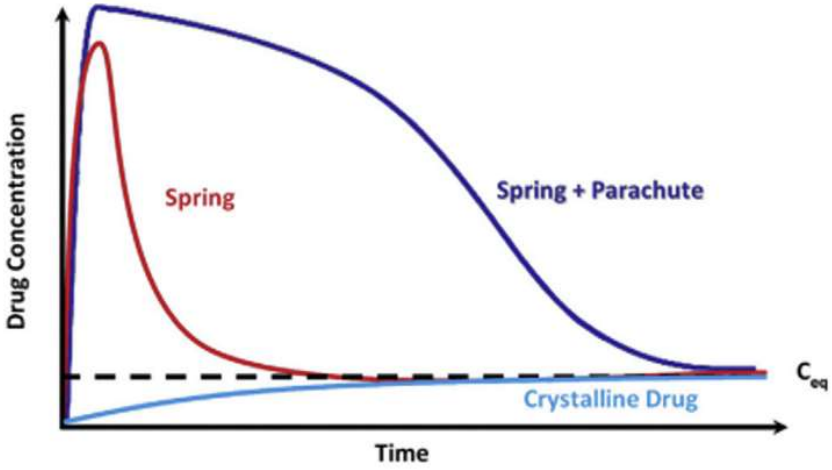

Figure 2-7: Spring and Parachute concept for the solubilization mechanism of PASDs [18]

Therefore, concerning PASDs, in the ideal case the drug first dissolves along with the polymer and forms a supersaturated solution (spring), after which the supersaturation should be maintained long enough to cause drug absorption (parachute). Three different mechanisms are possible for the dissolution behaviour of the drug differentiated by the release speed of polymer and drug and the morphological state of the drug after release, but a detailed description can be found elsewhere [18], [37].

A polymer used as a carrier in PASDs should be able to maintain the metastable amorphous state of the drug long enough to facilitate drug absorption and avoid precipitation of the drug [18]. Vinyl polymers and cellulose derivatives such as HPMC have been investigated as polymers that can prolong supersaturation and prohibit precipitation [37]. The mechanism behind that ability is not fully understood yet but might be related to drug-polymer interactions [18].

2.5.2 Controlled and Extended Drug Release

Controlled oral drug release in general aims to develop concepts to administer a specific dose of an API into various parts of the gastro-intestinal system in the body. Extended release is one form of controlled release with the goal to develop formulations that achieve specific drug concentrations within the therapeutic window over a prolonged time [45]. A graphical representation can be seen in *Figure 2-8*.

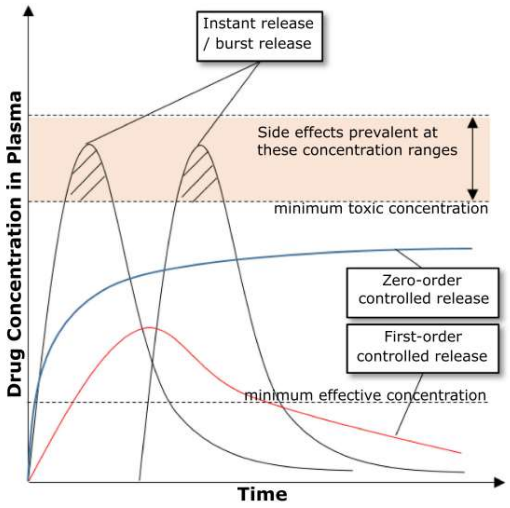

Figure 2-8: Schematic representation of extended drug release systems (blue and red line), which allow the concentration to be approximately constant in the plasma compared to repeated doses with instant or burst release systems [45]

The range between the minimum toxic concentration (MTC) and the minimum effective concentration (MEC) is the therapeutic window where an API has a positive therapeutic effect. Controlled, or extended release, formulations aim to design release profiles within this window, with several physical, chemical or biological factors that can trigger the drug release [45]. This design of delivery systems has significant therapeutic and economic benefits. They may lead to a reduction of the dose frequency and possible complications, and therefore reducing treatment burden and improving compliance. Furthermore, they reduce side effects and toxicity issues compared to several individual doses, as illustrated in *Figure 2-8* [12], [45].

The design of extended release profiles from formulations is based on the principal physical mechanisms relevant for drug dissolution. Since extended release is, by definition, a long process, accurate prediction and models are necessary. The applicability of these models strongly depends on the dominating release mechanism [45]. A classification concerning the mechanism controlling the drug release behaviour distinguishes between diffusion-controlled, chemically controlled, solvent-activated (e.g. swelling controlled systems) and modulated release systems. Furthermore, each of these categories can be divided into subcategories [12].

3 MATERIALS AND METHODS

This chapter contains the used methods and characterisation tools in the order in which they were performed as well as brief information on the used materials.

3.1 MATERIALS

As polymer carriers, the cellulose derivative hydroxypropyl methylcellulose (HPMC) and polylactic acid (PLA) are chosen. Naproxen is used as a model drug. The used HPMC is AFFINISOL™ HPMC HME 4M designed by DuPont, was purchased in form of a powder from Dow Wolff Cellulosics GmbH, Germany. It is tailored to increase the solubility requirement of novel APIs, while expanding the thermal processing window and additionally increasing the solubility in organic solvents. Furthermore, it has a significantly higher MW compared to other types of HPMC [34]. The PLA-pellets used in this work were purchased from NatureWorks Bioplastics, USA. Naproxen (NPX) was purchased in powder form from Sigma Aldrich (CAS-Nr.: 22204-53-1, Product-Nr: N8280). All materials were used as received.

3.2 METHODS

The manufacturing of the filaments as well as the different analysis methods are described in this chapter and process parameters as well as the design of the experiments are detailed.

3.2.1 Hot Melt Extrusion (HME)

For the manufacturing of the filaments, a co-rotating twin screw extruder (Micro-compounder Xplore MC5) with a chamber volume of 5 *ml* was used. A round die with a diameter of 1.75 *mm* and a conveyor belt were utilized to obtain straight and uniform filaments.

At first the extrusion temperatures were chosen within a processing window of 160-190 *°C* based on the thermomechanical properties of the used substances (cf. *Table 3-1*), which were already determined in previous works [46], [47].

Table 3-1: Thermodynamic properties of the pure components

Substance	T_g [°C]	T_m [°C]	T_d [°C]
PLA	60	150	351
HPMC	115	-	313
Naproxen	-	153	249

Theoretically the extrusion temperature should be above the melt temperature and significantly below the degradation temperature to process the mixture without damaging the components. However,

experiments showed that NPX has a significant influence on the melting temperature of the mixture, which resulted in processing temperatures below the melt temperatures of the pure components for some formulations.

For every formulation a total of 5 *g* of polymer-drug mixture was manually fed into the barrel at 180 °*C* and varying screw speeds, depending on the formulation. Afterwards the components were mixed at this temperature for 5 or 10 *min* for pure polymer mixtures and mixtures with NPX respectively, before the mixture was extruded. For the ternary formulations half of the PLA content was always added first to reduce the friction between the material and the extruder barrel, because PLA has the best thermomechanical properties. Afterwards HMPC and NPX were added alternately. The exact extrusion parameters for the different formulations can be found in *Chapter 4.2*. After the extrusion process the filaments were stored in sealed plastic bags at room temperature.

3.2.2 Dynamic Scattering Calorimetry (DSC)

To characterise the thermodynamic properties of the filaments, DSC was carried out in a Mettler-Toledo DSC 2 STAR^e System as well as a DSC 250 from TA instruments. All formulations, as well as the pure components, were analysed in the form of extruded filaments, except for NPX which was analysed as powder. For the analysis approximately 5 *mg* pieces were cut from the filaments with a scalpel and weighed in a 40 *µl* aluminium pan. Subsequently, the pan was closed and sealed with a pierced aluminium lid to reduce losses during the analysis. For the measurement, the pan was placed into the autosampler and the analysis was performed automatically by the software according to an individually programmed heating cycle. Measurements were performed at inert conditions with a nitrogen flowrate of 50 *ml/min*. The used cycle was the same as in a previous study [47] to ensure comparability of the results. It consisted of two heating cycles and a cooling cycle in between with a heating and cooling rate of 10 *K/min,* respectively:

(i) 1min: 0 °*C* Isothermal
(ii) 0 °*C* – 200 °*C*
(iii) 1min: 200 °*C* Isothermal
(iv) 200 °*C* – 0 °*C*
(v) 1min: 0 °*C* Isothermal
(vi) 0 °*C* – 200 °*C*

The first cycle can give insight on the processing of the material and was furthermore used to erase any remaining thermal history. The second heating cycle provides information about the material itself and was used for characterisation.

To determine the T_g from the DSC curves the Mettler Toledo Star^e Evaluation software was used and with the 'Step-Tangent'-tool the T_g is determined as the resulting inflection point of the endothermic shift. However, it should be mentioned that there are several suggested ways shown in literature to determine the T_g, because the glass transition is a region rather than a precise temperature [32]. The inflection point is chosen over the onset- or the midpoint because the T_g can be determined more accurately. The onset- or midpoint, which can also be determined with this tool, depend on the place of the drawn evaluation points, and therefore change with each evaluation.

3.2.3 Wide Angle X-Ray Scattering (WAXS)

To investigate the degree of crystallinity and i.e. if ASDs were formed during HME, the filaments were investigated with WAXS using a Mat:Nordic SAXS Unit (SAXSLAB) with a Copper K-α X-ray energy source. In the first step, the detector was calibrated against silver behenate (AgBeh). Subsequently, the filaments were taped onto the sample holder to keep them in a fixed position. The exact alignment of the filaments for the measurement was done by using the software to determine the position that causes the highest response (usually in the middle of the filament). The measurement time was set to 5 *min* to obtain distinct scattering curves.

3.2.4 ATR-FTIR Spectroscopy

To analyse interactions between the components, ATR-FTIR spectroscopy was carried out with a Perkin Elmer Frontier IR/FIR with a specialized ATR accessory (Far-IR ATR). The spectra were obtained at room temperature in the range between 400-4000 cm^{-1} and 20 scans at a resolution of 4 cm^{-1}. In the first step a background spectrum was recorded. In this measurement it was important not to apply pressure by the sample holder yet, because the spectrum should be conducted on air. Afterwards, the filaments were placed onto the ATR-crystal and fixed with the sample holder. All investigated formulations, as well as the pure polymer samples, were analysed in the form of extruded filaments, except for NPX which was analysed as a powder.

3.2.5 Raman Spectroscopy

Raman mapping was performed on the extruded filaments on a confocal Raman microscope (LabRAM HR Evolution from Horiba Scientific). To analyse the filaments, a smooth surface is necessary and therefore the pieces were cut with a special cutter (LEICA EM TXP). For the measurement, the pieces were fixed perpendicular to the glass slide in a small metal sample holder. A 633 *nm* laser (red) at 100 % intensity was used to reduce the high luminescence of HPMC. Furthermore,

an objective lens with 50x magnification and 0.5 numerical aperture was utilized. The mapping was performed with an acquisition time of 4 *sec*, an accumulation of 2 and a pinhole size of 50 *µm*. An approximately 50x50 *µm* rectangle was measured on the filaments cross-sectional surface with a resolution of 1 *point*/*µm*.

3.2.6 Dissolution Studies

The produced filaments were tested quantitatively with in vitro dissolution studies. The experiments were carried out in standard USP dissolution apparatuses at 37 *°C* in phosphate buffer (0.1 *M*, pH 6.8), in an attempt to simulate human body temperature and intestinal fluids [48]. The filament pieces (properties see *Chapter 4.7*) were put into round bottom USP baths with a buffer volume of 900 *ml,* with the position of the paddle-stirrers adjusted approximately 2.5 *cm* above the bottom of the container and the stirring speed set to 50 *rpm*. Since the filaments are not floating, no baskets were used, and the pieces could flow freely on the bottom of the containers, which were closed with special lids to reduce evaporation losses.

Different sizes of filament pieces were used for 10 wt.% drug and 30 wt.% drug samples, respectively. 50 *mg* pieces were used for lower drug content, and 15 *mg* pieces for higher drug content, to stay below the solubility limit of the drug. For the first two hours of all experiments, samples were taken every 30 *min* to detect a possible burst release. After this period the sampling interval was adjusted based on the observed release speed and ranges from every hour to every other day, depending on the investigated formulation.

For each sampling point 2 *ml* were taken from the respective release baths with a micropipette and subsequently 2 *ml* of buffer were added to ensure a constant volume. For release experiments which lasted longer than a week, deionised water was added to compensate evaporation losses. This included taking a sample, before and after the addition of deionised water, to correct the new concentration accordingly. All samples were analysed via UV-Vis spectroscopy to determine the concentration of NPX in the phosphate buffer.

3.2.6.1 UV-VIS Spectroscopy

The measurements were carried out in a UV-Vis spectrometer (Agilent Cary 60, Version 2) using a 3 *ml* quartz cuvette with a path length of 10 *mm*. For the analysis of the samples a calibration curve is needed to correlate the absorption of the drug to the concentration. The used calibration curve for Naproxen can be found in the Appendix (cf. *Figure 7-1*). For all samples a baseline correction with pure phosphate

buffer was determined. The samples were investigated between 200-800 *nm* wavelength and a scanning rate of 4800 *nm/min*. The maximum absorbance of Naproxen was determined at a wavelength of 231 *nm* and values to calculate the concentration were taken at this distinctive peak.

3.2.7 Scanning Electron Microscopy (SEM)

Filament pieces after release were analysed with SEM (Zeiss Ultra 55 FEG SEM). Since this method is not suitable for samples with high water content the samples had to be prepared before the analysis. After the pieces were taken out of the release baths, the samples were stored in falcon tubes filled with buffer to prohibit natural drying of the samples. To avoid changing the morphology of the pieces, the samples were frozen with liquid nitrogen for approximately 20 *sec*. Subsequently, they were put into microcentrifuge tubes and submerged into an ice bath and then vacuum freeze dried for 72 *h*. Since samples analysed with SEM additionally need to be conductive, they were sputtered with gold (~ 10 *nm* layer). Afterwards, the filaments were broken in half to obtain pictures of the cross-section. The samples were analysed with a secondary electron detector at a voltage of 3 *kV*.

4 RESULTS AND DISCUSSION

The results obtained with qualitative and quantitative analysis methods of the extruded filaments and their interpretation are described in detail in this chapter. First, the miscibility assessment and the characterisation of the extruded filaments are described. Afterwards, the analysis with DSC, WAXS and ATR-FTIR spectroscopy as well as Raman mapping, prior to the in vitro studies, is outlined. Furthermore, the release curves generated with in vitro dissolution studies are analysed, and the resulting SEM images of the remaining PLA matrix after release are shown.

4.1 ESTIMATION OF MISCIBILITY AND INTERACTION

A theoretical estimation of the thermodynamic miscibility and the interaction of two polymers or between drug and polymer can be made by the determination of the HSP and the so-called 'distance' between two substances. The values for the three components are obtained from literature and stated in *Table 4-1*.

Table 4-1: Hansen solubility parameters of the investigated substances PLA [42]*, NPX* [49]*, HPMC* [34]

Compound	δ_D [MPa$^{1/2}$]	δ_P [MPa$^{1/2}$]	δ_H [MPa$^{1/2}$]
PLA	18.6	9.9	6
NPX	17.4	12.1	9.6
HPMC	17.8	11.4	12.7

For a better visualization the HSP are also plotted according to the 'Hansen-Space' in *Figure* 4-1 with a radius of 10.7 for PLA [40]. The 3D plot shows that HPMC, as well as NPX, are located within the sphere of PLA. While polymer compatibility is usually assessed by the overlap of two polymer spheres, this already shows that the two polymers, as well as the drug and each polymer, are sufficiently 'alike' and therefore should be compatible. However, that does not mean that the two polymers cannot phase separate [40].

Furthermore, to estimate the solubility of a drug in a polymer or the similarity between two polymers [40], [42], the distance of the compounds can be calculated from their individual HSP (cf. *Chapter 2.4.4*). The calculations result in 4.9 for PLA/NPX, 3.3 for HPMC/NPX and 7.0 for PLA/HPMC, indicating that NPX prefers HPMC over PLA, which is confirmed with experiments later. The short distance between the polymers and the API indicates that the drug is soluble in both polymers and not likely to precipitate [40], [42].

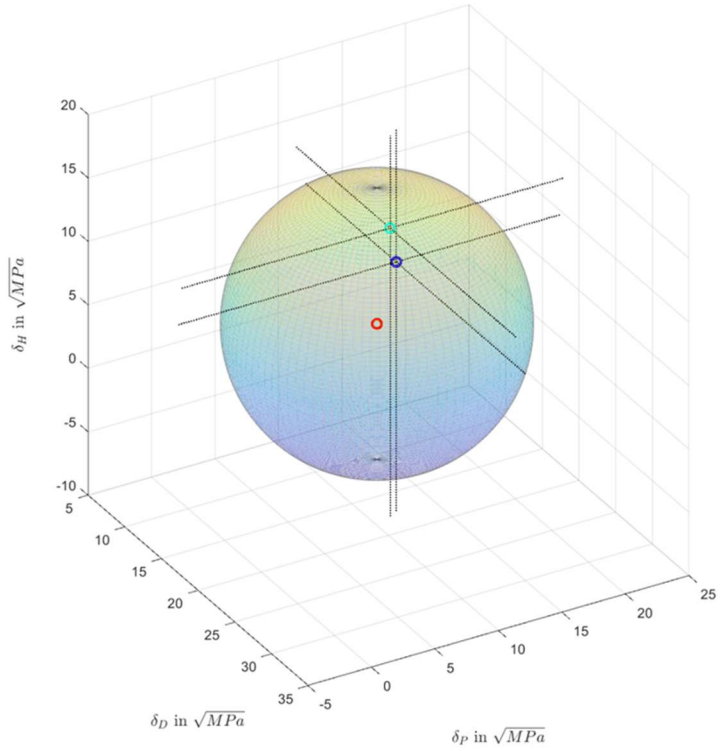

Figure 4-1: Solubility sphere of PLA (radius=10.7) with the respective positions of PLA (red), NPX (blue) and HPMC (green)

Overall, these results indicate that the formulation and blend of this ternary formulation is possible in theory. Furthermore, this analysis provides a valuable assessment in formulation development to determine suitable compounds.

4.2 CHARACTERISATION OF THE EXTRUDED FILAMENTS

To investigate the phase behaviour of PLA, HPMC and the drug NPX different formulations are produced. The API content (10 or 30 wt.%) is calculated based on the total mass of the mixture (for 5 *g* mixture this means 0.5 & 1.5 *g* NPX, respectively). The remaining weight percent of the mixture consists either of only one polymer or the two polymers in a specific ratio. Concerning the nomenclature of the different formulations in this thesis, the labelling of the samples contains the polymer weight ratio always in the order PLA:HPMC, following the overall drug content (if any) in wt.%. *Table 4-2* provides an overview of the sample names with the respective weight percent regarding the total mass of the mixture. All the investigated formulations are additionally depicted in *Table 4-3* with their respective extrusion parameters.

Table 4-2: Overview of the nomenclature and the corresponding weight percent

Formulation Name	wt.% PLA	wt.% HPMC	wt.% NPX
70:30	70	30	-
50:50	50	50	-
30:70	30	70	-
PLA_10 wt.% NPX	100	-	10
PLA_30 wt.% NPX	100	-	30
70:30_10 wt.% NPX	63	27	10
70:30_30 wt.% NPX	49	21	30
50:50_10 wt.% NPX	45	45	10
50:50_30 wt.% NPX	35	35	30
30:70_10 wt.% NPX	27	63	10
30:70_30 wt.% NPX	21	49	30
HMPC_10 wt.% NPX	-	100	10
HPMC_30 wt.% NPX	-	100	30

Table 4-3: Extrusion parameters for all investigated formulations

Formulation Name	Mixing Time [min]	Mixing Speed [rpm]	Extrusion Speed [rpm]	Extrusion Temperature [°C]
Pure PLA	5	50	50	180
70:30	5	50	50	180
50:50	5	50	50	180
30:70	5	50	50	180
Pure HPMC	5	50	50	180
PLA_10 wt.% NPX	10	50	50	165
PLA_30 wt.% NPX	10	50	50	150
70:30_10 wt.% NPX	10	50	20	165
70:30_30 wt.% NPX	10	75	20	130
50:50_10 wt.% NPX	10	50	20	165
50:50_30 wt.% NPX	10	75	20	130
30:70_10 wt.% NPX	10	75	100	180
30:70_30 wt.% NPX	10	75	100	170
HMPC_10 wt.% NPX	10	75	100	180
HPMC_30 wt.% NPX	10	50	50	185

The extrusion parameters (temperature and screw speed) must be adjusted depending on the formulation to produce satisfying properties of the mixture regarding extruding a straight uniform filament. This means they should neither be too solid to cause insufficient mixing, nor too liquid and trickling out of the barrel. Notice that the mixing temperature of 180 $°C$ is the same for all formulations.

4.2.1 Filaments with Different PLA:HPMC-Ratios

Initially, formulations without NPX were extruded, to test the behaviour of the hydrophobic PLA and the hydrophilic HPMC polymer during extrusion. The samples were all extruded at the same process parameters (mixing: 50 *rpm* for 5 *min* and extruding: 180 °*C* and 50 *rpm*). Although pure PLA is slightly softer and has a lower viscosity than HPMC at this extrusion temperature, satisfying results were obtained with these parameters, regardless of the polymer ratio. This suggests no strong interaction between the two polymers since the processing temperature, i.e. the melting and glass transition temperature for the mixtures seem to be only slightly influenced, at least upon visual inspection (further details see *Chapter 4.3*). In *Figure 4-2* pieces of the filaments for the investigated polymer mixtures can be seen.

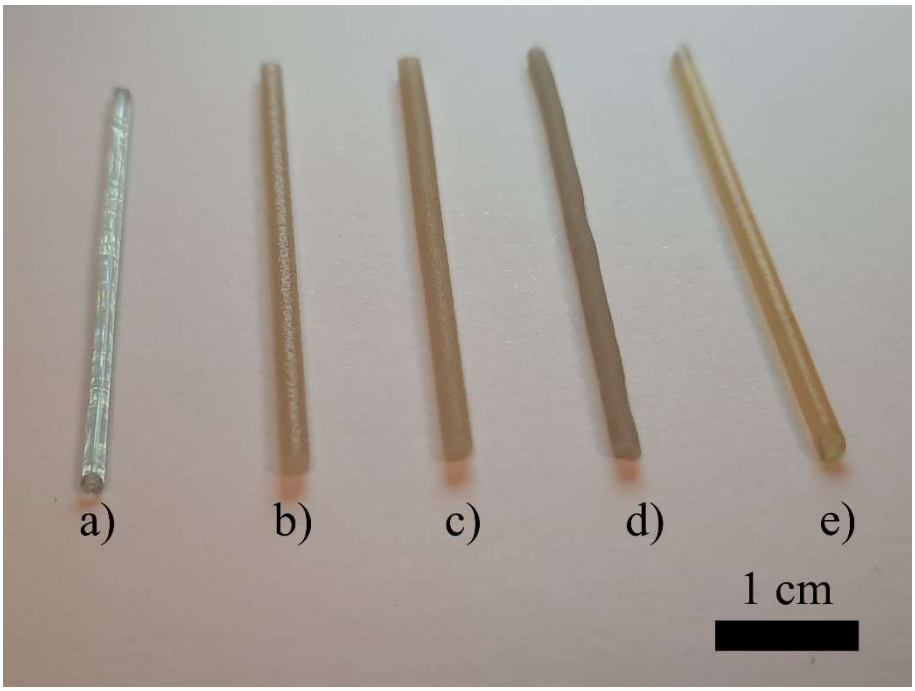

Figure 4-2: Filaments without NPX; polymer ratios: a) pure PLA; b) 70:30; c) 50:50; d) 30:70; e) pure HPMC

All filaments have a smooth surface, appear homogenous and could be extruded as a straight filament. Pure PLA (a) is transparent and translucent and has a slightly smaller diameter than the other samples, either due to a possible lower viscosity or melt shrinkage of PLA. Pure HPMC (e) is also translucent and has a light brown/yellow colour. The filaments containing a polymer mixture (b, c, d) are not translucent and have a beige or light brown colour. The shape of the mixture with the lowest PLA content (d) shows irregularities and slight grey colouring. Experience with this extruder suggests that this grey colouring is caused by too high friction in the barrel and leads to fouling. Too high friction appears for example if the mixture in the barrel is too solid to be properly processed.

4.2.2 Filaments Containing 10 wt.% NPX

The extrusion parameters for the formulations containing NPX do not suggest a strong influence of the composition anymore. Considering the various process parameters and their combinations for the investigated formulations (cf. *Table 4-3*), complex synergistic effects between the polymers and drug are observed and they do not follow any clear trend solely influenced by the weight percentage of the substances.

For all samples containing NPX is seems, to ensure sufficient mixing, the mixing time must be increased compared to corresponding formulations without API. If this is not considered, the filaments appear inhomogeneous with varying viscosities during the extrusion period. After the increased mixing time, a visual inspection indicates that the filaments become homogenous and sufficiently mixed on a macroscale.

Additionally, as previously stated, the extrusion temperature must be adjusted depending on the formulation. Theoretically the temperature should be chosen within the previously investigated processing window, i.e. depending on the melting and degradation temperature of the pure components. The adjustment of the temperature, however, is based on a trial and error approach since it proves to be challenging to predict the temperature to produce a desirable consistency for extrusion by only taking the weight percentage of the different substances into account.

The results for formulations containing 10 wt.% NPX are depicted in *Figure 4-3*. The addition of API for high PLA percentage (a, b) seems to have no influence on the colour and the appearance of the filaments compared to the mixtures without drug. However, with increasing HPMC percentage (c, d) the filaments seem slightly darker, suggesting possible fouling inside the extrusion barrel due to higher friction.

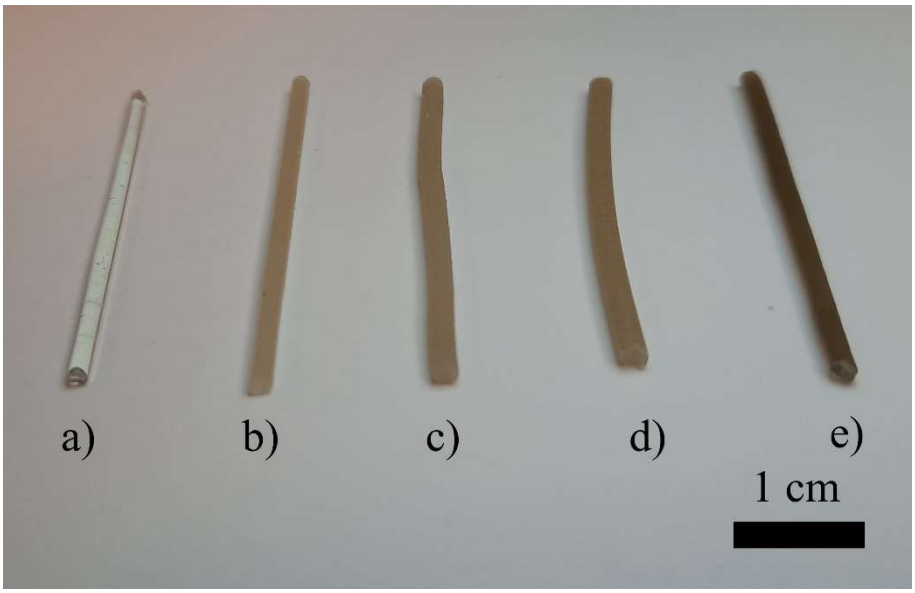

Figure 4-3: Filaments with 10 wt.% NPX; polymer ratios: a) PLA; b) 70:30; c) 50:50; d) 30:70; e) HPMC

It was also observed for formulations containing API that it was more difficult to get perfectly straight extruded filaments with a narrow diameter variation along the filament, probably because the extrudates leave the die very slowly.

The filament containing only HPMC and NPX (e) has a grey colour, indicating too high friction in the barrel. Since a further increased temperature would have led to degradation of the drug, this discolouration of the filament was accepted.

4.2.3 Filaments Containing 30 wt.% NPX

The mixtures containing 30 wt.% drug (cf. *Figure 4-4*) were proven to be the most difficult for HME. For two formulations (b, c), the investigated processing window is not suitable and to produce homogenous filaments the extrusion temperature had to be lowered to 130 °*C* (20 °*C* below the lowest melt temperature of the pure components). When evaluating the results for the 50:50 formulation (c), it should be remembered that some degradation might have occurred, even though a low extrusion temperature was used.

For pure PLA with 30 wt.% NPX (a), indications of a significant plasticizing effect of the API were observed since the mixture could be extruded 30 °*C* below the temperature of pure PLA. In addition, the filament has a smaller diameter (because of this formulation´s low viscosity). Further details on the varying diameters of the filaments can be found in *Chapter 4.7*. Combined with the observation that

formulations with high PLA and low HPMC percentage must be extruded at even lower temperatures this supports the theory of NPX having a strong plasticizing effect on PLA.

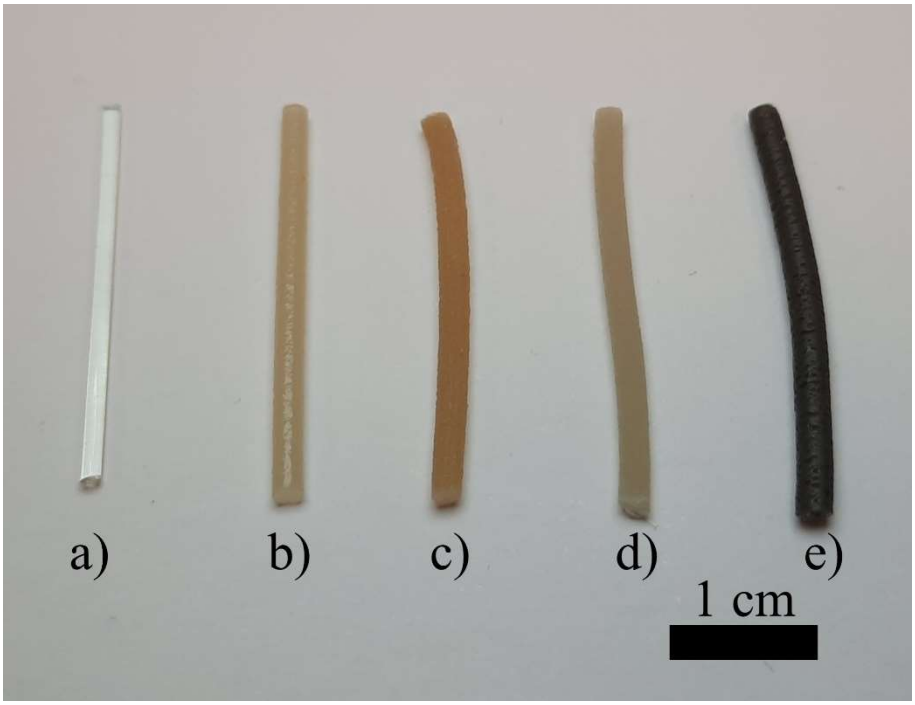

Figure 4-4: Filaments with 30 wt.% NPX; polymer ratios: a) PLA; b) 70:30; c) 50:50; d) 30:70; e) HPMC

Concerning formulations with high HPMC content (d), or only HPMC (e), an opposite tendency is observed. These formulations were extruded at the same temperature than the pure components, but with an increased extrusion speed, and still the extrudate, immediately solidify after exiting the die. For the 30:70 polymer ratio (d) the adjustment of the extrusion speed was successful but showed significant degradation of the API for the composition with only HPMC and 30 wt.% NPX (e), resulting in a completely black filament. One possible explanation for the black filaments could be that HPMC interacts with NPX, causing an increased viscosity of the mixture and thus leading to high friction inside the barrel.

These results proof that the understanding of polymer-polymer and polymer-drug interactions is of great importance to successfully produce filaments via HME containing more than one substance. Because the extrusion process is time-consuming, not all possible parameter combinations could be tested within this work. Thus, a future goal to get beyond a trial and error approach for the extrusion parameters could be to create tools to predict suitable process parameters for different formulations, and by that reduce waste and save time in the development of new formulations intended for HME.

4.3 THERMAL CHARACTERISATION

After extrusion, the filaments were analysed quantitatively to get insight into the phase behaviour of the components. Knowledge about the glass transition region for polymer mixtures gives an indication about the miscibility of the polymers. Therefore, a DSC analysis is performed on all the filaments as well as on NPX powder. Furthermore, the T_g is additionally determined via the Gordon-Taylor Equation.

First the polymer mixtures without any NPX are compared. *Figure 4-5* depicts the DSC results of the second heating cycle for the pure components and for the different polymer ratios. Here it should be mentioned that there were DSC software issues with the DSC used for the analysis in the first place and the generated thermograms showed unrealistic and oscillating curves for some formulations. Hence several formulations were analysed again with another DSC instrument to validate the results, but due to time limitations not all formulations were analysed again. The new obtained curves show the same glass transition, but do not show the unrealistic and oscillating behaviour, suggesting that they were caused by software issues of the instrument and not the material. The formulations measured with the first DSC have no label, the ones measured with the second DSC are indicated with a dot (•), and the measurements used from previous works are labelled with a star (*).

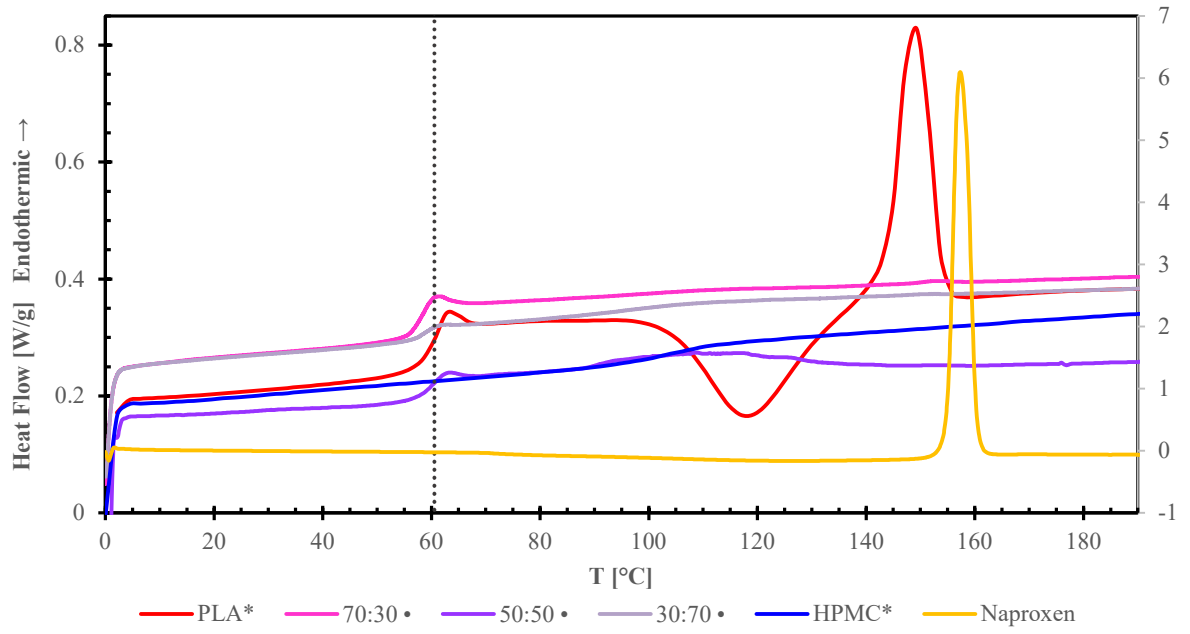

Figure 4-5: DSC curves of the second heating cycle for the pure components as well as the investigated formulations with a mixture of PLA and HPMC; data marked with a star is obtained from a previous work [47]*; data marked with a dot is obtained on another DSC device; the curve for Naproxen is scaled on the secondary axis (right side)*

Pure PLA (red) displays a clear glass transition at approx. 60 °C, a small melt peak at 153 °C, as well as a cold crystallisation peak at approx. 120 °C. The dotted line represents the determined glass transition

temperature for PLA. A glass transition temperature of approx. 60 °*C* also aligns with literature for PLA with high MW [50]. Pure HPMC does not display a distinct transition peak but rather a wide transition range, and as shown in the literature, a T_g around 115 °*C* can be stated [34]. Naproxen displays a clear melt peak at approx. 156 °*C* and a glass transition at approx. 3.5 °*C* (not visible due to the scale of the diagram), which is slightly lower than shown in the literature before [51].

Results for the different polymer mixtures clearly show almost the same T_g compared to pure PLA and a slight endothermic shift in the vicinity of the T_g of pure HPMC. A comparison of the results obtained with DSC and the theoretical T_g calculated with Gordon-Taylor can be found in *Table 4-4*. The densities used for the calculation of the Gordon-Taylor constant are 1.25 g/cm^3 for NPX [51], 1.2 g/cm^3 for HPMC [34] and *1.252* g/cm^3 for PLA [36].

Table 4-4: Comparison of the glass transition obtained with DSC measurements and theoretically calculated with the Gordon-Taylor equation

Polymer Ratio	T_g [°C]	
	Gordon Taylor	DSC
PLA	-	60.7
70:30	70.3	60.2
50:50	78.9	60.5
30:70	90.1	61.0
HPMC	-	115
PLA_10 wt.% NPX	22.1	51
70:30_10 wt.% NPX	66.8	54.2
50:50_10 wt.% NPX	79.4	56.0
30:70_10 wt.% NPX	87.3	55.3
HMPC_10 wt.% NPX	25.4	146.3
PLA_30 wt.% NPX	9.6	36.8
70:30_30 wt.% NPX	34.1	42.0
50:50_30 wt.% NPX	45.3	45.0
30:70_30 wt.% NPX	53.9	48.5
HPMC_30 wt.% NPX	9.9	158.2

The results clearly indicate that the T_g is not influenced by the composition of the polymer mixture and that the glass transition does not follow the Gordon-Taylor Equation at all. This suggests that the two phases are indeed phase separated. The mixture should additionally show a second T_g close to the one of HPMC, but since the transition is already hardly visible for the pure component no second glass transition could not be detected clearly with the DSC.

Upon the addition of NPX to PLA however, the T_g is clearly influenced. In *Figure 4-6,* the results of the formulations containing only one polymer and the API are shown. Here it becomes clear that NPX has a strong plasticizing effect on PLA, as already indicated during the extrusion process. The addition of 30 wt.% NPX reduces the T_g of the mixture by approx. 24 °*C*. However, for HPMC there might even be anti-plasticization indicated by the endothermic shift at approx. 158 °*C,* which could explain the fouling of the extruder due to a too high viscosity of the mixture within the investigated processing window. This evident influence of NPX on PLA, as well as on HPMC, further suggests that the drug can be incorporated in both polymers.

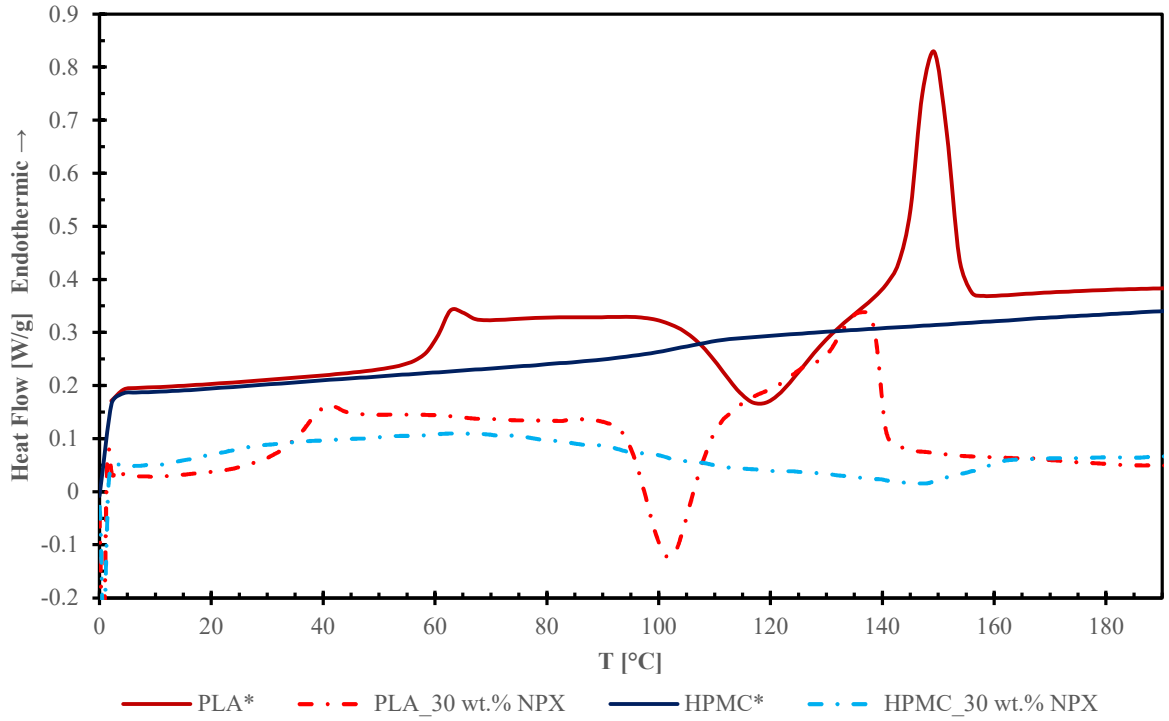

Figure 4-6: DSC curves of the second heating cycle detailing the influence of NPX on PLA and HPMC; without NPX (full); 30 wt.% NPX (dot dashed); data marked with a star taken from a previous work [47]

A similar plasticizing effect could be observed for the ternary formulations shown in *Figure 4-7,* for mixtures with different polymer ratios and drug contents. Already the addition of 10 wt.% NPX leads to a significant decrease in T_g of about 16 °*C* for all polymer ratios and indicates a plasticizing effect on the polymer mixture, resulting in a T_g of approx. 54 °*C*. This shows that for this low drug content, the amount of PLA is not crucial for the plasticization effect.

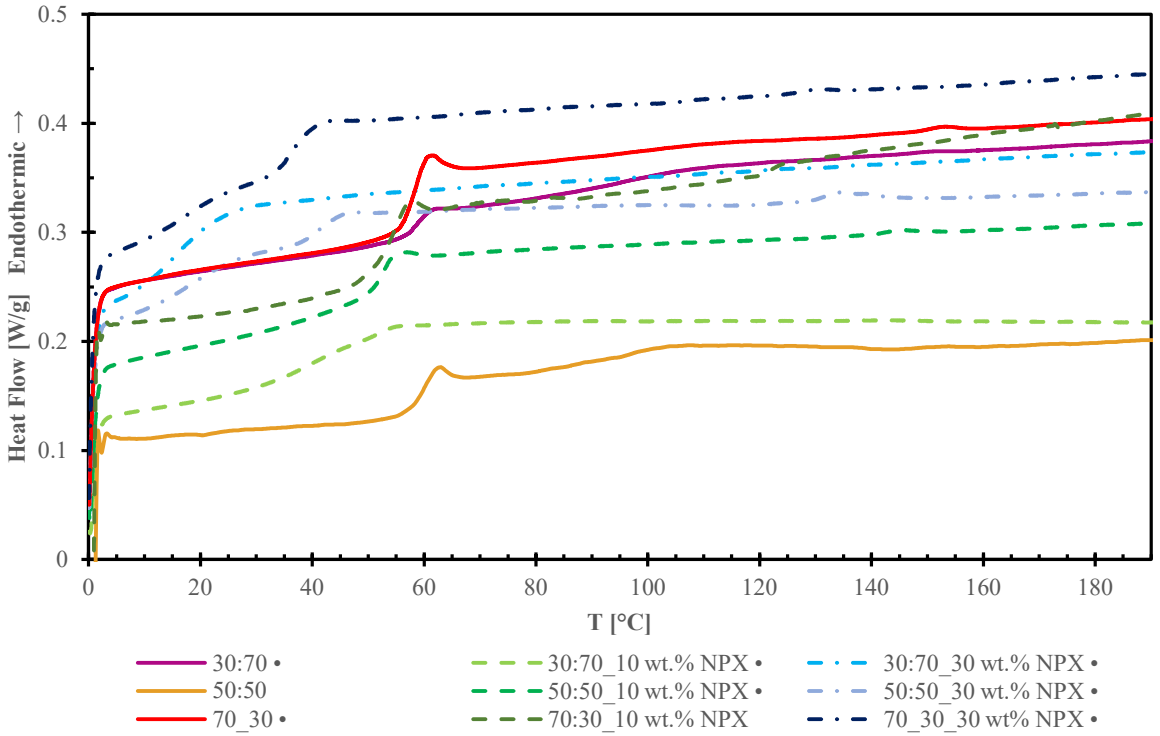

Figure 4-7: DSC curves of the second heating cycle for all the investigated formulations with different polymer ratios and drug contents; without NPX (full); 10 wt.% NPX (dashed); 30 wt.% NPX (dot dashed); data marked with a dot is obtained on another DSC device

For 30 wt.% drug content, the decrease in T_g is influenced by the polymer ratio and decreases more significantly for higher PLA percentages, resulting in glass transition temperatures of approximately 48.5 °*C* for a polymer ratio of 30:70, 45 °*C* for 50:50 and 42 °*C* for 70:30. These values are consistent with the observations during extrusion where NPX appeared to have a more significant plasticization effect on PLA than on HPMC, where even an indication of an anti-plasticization effect of NPX, and an increase of the viscosity were observed.

Overall, the results indicate a phase separated system of the two polymers and show a significant plasticizing effect of NPX for PLA, but not for HPMC. Additionally, the DSC analysis shows that the changes in the glass transition are complex and hard to predict before extruding.

4.4 POLYMER MORPHOLOGY

Because ASDs increase the solubility of low solubility drugs, WAXS is performed to determine if an ASD was formed during extrusion. With scattering of X-ray waves, caused by differences in the electron density, structural information can be obtained [14]. The results for the pure components and binary polymer mixtures are shown in *Figure 4-8*.

The curves are presented as logarithmic plots of the absolute intensity of the scattering times the thickness of the sample (y-axis) over the scattering vector q (x-axis). The scattering vector corresponds to the scattering angle 2Θ, according to *Equation 4-1*, where λ is the wavelength of the X-ray beam and d the spacing between the scattering objects in the material according to Bragg's law.

$$q = \frac{4\pi}{\lambda} \cdot \sin\left(\frac{2\theta}{2}\right) = \frac{2\pi}{d} \qquad 4\text{-}1$$

Because the filaments are all very similar in size and composition, the scattering intensity is in the same range for all the formulations, and the original curves overlap, therefore the curves are arbitrarily aligned on the y-axis to distinguish the different curves. Crystalline structures like the analysed Naproxen powder show clear crystalline peaks, so called Bragg-peaks. The pure polymer filaments and the binary filaments only show broad peaks, so-called amorphous halos.

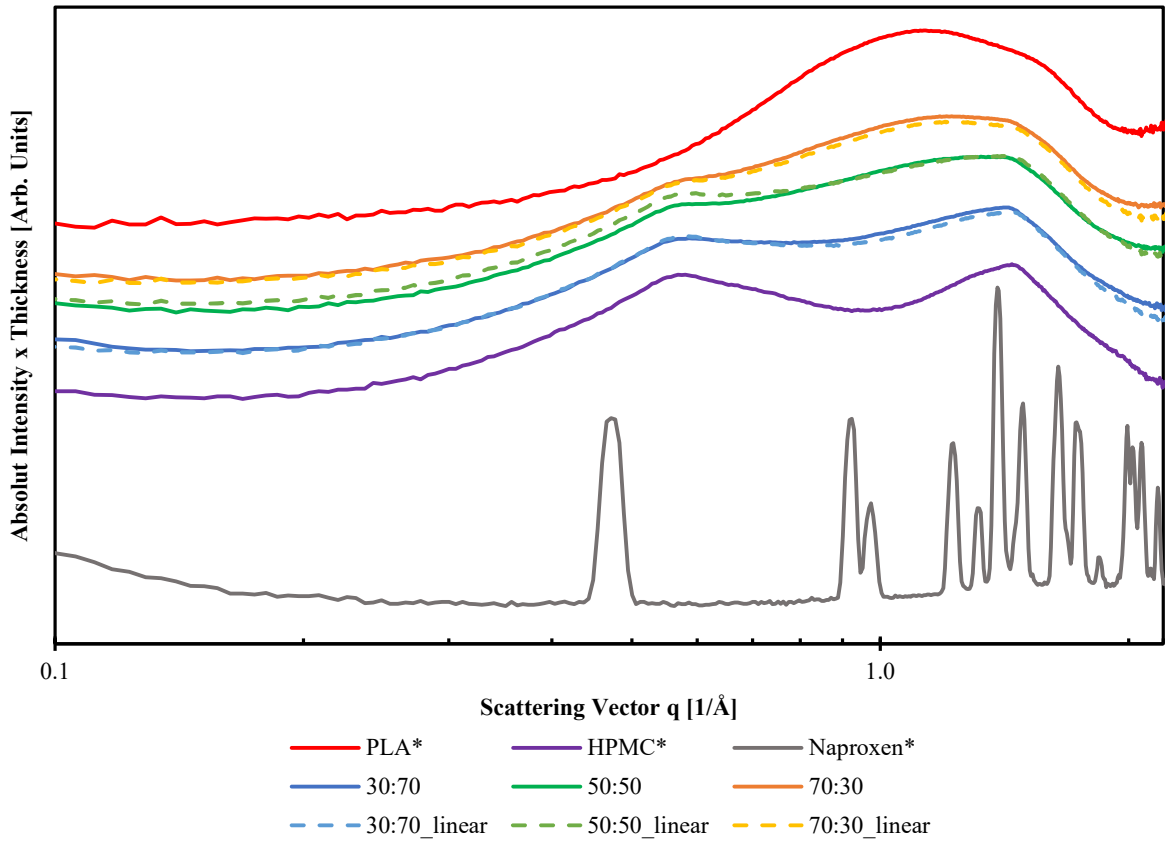

Figure 4-8: WAXS curves for the pure components and different PLA:HPMC ratios (pure component data marked with a star taken from a previous work [47]*); the different curves are arbitrarily aligned on the y-axis for better visualization, and the dashed lines represent calculated linear combinations of the pure components in the respective ratio*

The dashed lines in the diagram represent calculated linear combinations of the pure polymer data in the respective ratio. The comparison of the calculated curves (dashed lines) and the measured curves (full

lines) display an almost perfect alignment. This suggests that the two phases are indeed present in separated areas and scatter according to their respective intensity and therefore the spectra are just a linear combination.

In general, PLA displays only one broad peak, whether HPMC shows two amorphous peaks. For the different binary mixtures, depending on the HPMC content, the two peaks are either more pronounced or less distinct in the case of the 70:30 ratio, reflecting on the different compositions.

In the next step, the incorporation of NPX into the mixtures was investigated for the binary polymer mixtures, which is shown in *Figure 4-9*, where the pure components are also depicted as references. The analysis clearly shows that the Bragg-peaks vanish if NPX is incorporated into the polymer mixture for all the formulations, demonstrating that the API is present in an amorphous state and no crystalline NPX is present. For low drug content, there is almost no change in the curve compared to the binary mixtures, but for 30 wt.% NPX the curves get slightly smoother, and the peaks become flatter. A lack of crystalline peaks and the broad curves suggest that ASD were produced by HME for all investigated compositions. These findings align very well with the results obtained via DSC.

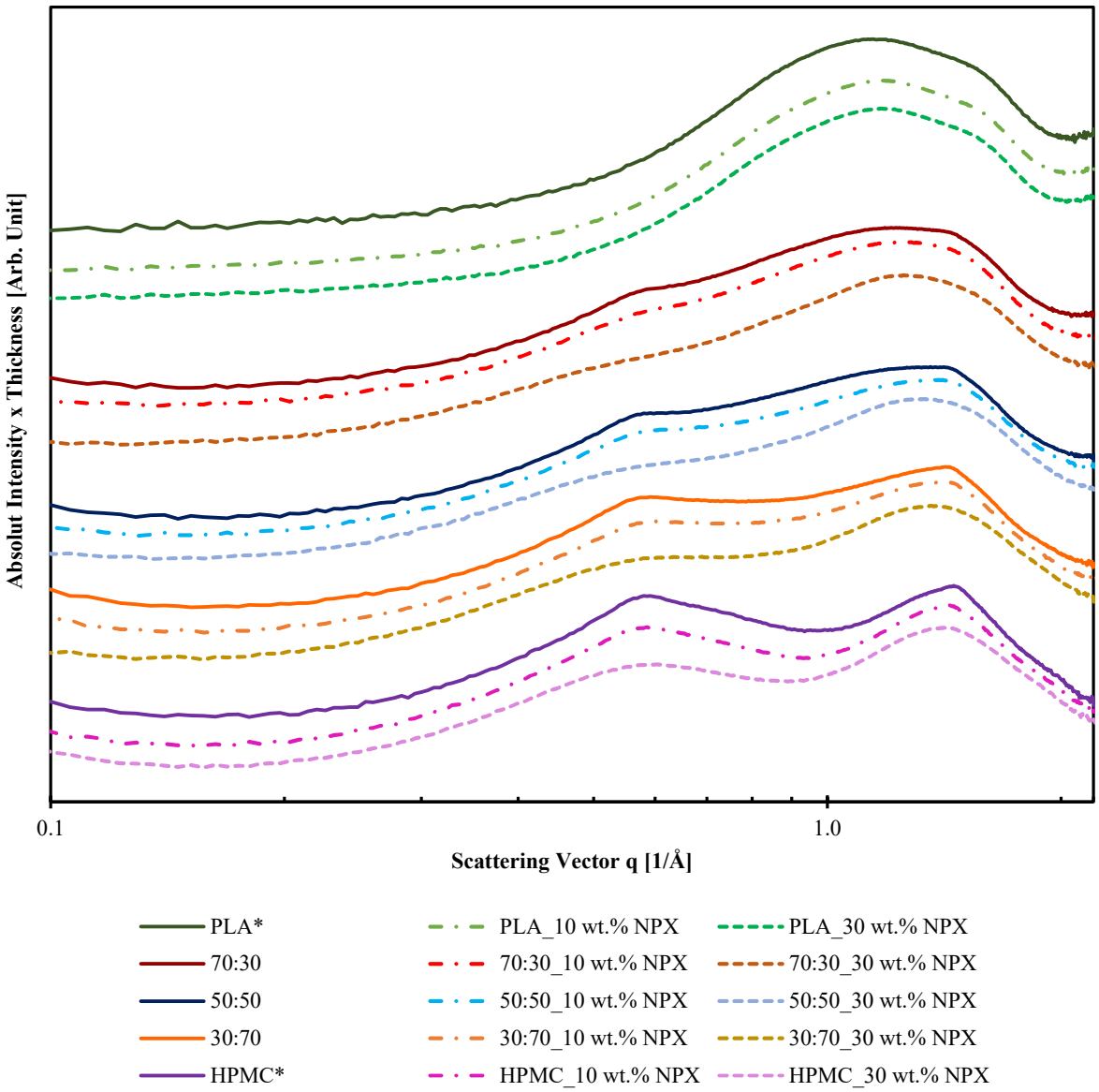

Figure 4-9: WAXS curves for the investigated formulations containing API; 10 wt.% NPX (full) and 30 wt.% NPX (dashed); pure component data marked with a star taken from a previous work [47]*; the different spectra are arbitrarily aligned on the y-axis for better visualization*

Because the WAXS analysis shows a successful formation of ASDs for all the formulations, a faster dissolution of the drug than in the crystalline state is possible. This result is quantitatively verified with release studies (cf. *Chapter 4.7*).

4.5 CHEMICAL STRUCTURE AND MODIFICATION

The internal molecular structure can be determined by investigating band vibration by using ATR-FTIR spectroscopy, which is a powerful tool to determine the nature and extend of drug-polymer interactions in solid dispersions [18], [52]. To provide an overview of the present functional groups, assigned IR-peaks are listed in *Table 4-5* to *4-7*. The values are taken from the listed references, where the

characteristic peaks were summarized from literature reviews. Changes in the structure or interactions of components can be detected by shifts in the frequency of the absorbance or changes in the relative intensity.

Table 4-5: Peak band assignment for PLA [50]

Assignment	Peak position [1/cm]
$-\mathbf{OH}$ stretch (free)	3571
$-\mathbf{CH}-$ stretch	2995
$-\mathbf{C}=\mathbf{O}$ carbonly stretch	1759
$-\mathbf{CH_3}$ bend	1453
$-\mathbf{CH}-$ deformation	1382,1362
$-\mathbf{C}=\mathbf{O}$ bend	1268
$-\mathbf{C}-\mathbf{O}-$ stretch	1194, 1130, 1093
$-\mathbf{OH}$ bend	1047
$-\mathbf{C}-\mathbf{C}-$ stretch	926,868

Table 4-6: Peak band assignment for crystalline/partially amorphous NPX [52]

Assignment	Peak position [1/cm]
$\mathbf{C}=\mathbf{O}$ stretching of non-H-bonded $-\mathbf{COOH}$	1718–1728
$\mathbf{C}=\mathbf{O}$ stretching of the H-bonded $-\mathbf{COOH}$	1681–1686
Aromatic stretching band of the naphthalene ring	1604
Bend/stretch and stretch/bend vibration band of free $-\mathbf{COOH}$, Respectively	1394 and 1260
$\mathbf{O}-\mathbf{H}$ stretching band of free and intermolecularly H-bonded naproxen, respectively	3196 and 2670

Table 4-7: Peak band assignment for HPMC [53]

Assignment	Peak position [1/cm]
$\mathbf{OH}$ stretching	3400
$\mathbf{C}-\mathbf{H}$ symmetric and asymmetric valence vibrations from $\mathbf{CH_3}$	3000–2800
$\mathbf{C}=\mathbf{O}$ stretching or deformation, $\mathbf{O}-\mathbf{CO}$ stretching	1760–1750
$\mathbf{CH_3}$ symmetric bending, $\mathbf{CH}$ bending, $\mathbf{C}-\mathbf{CH_3}$ stretching	1383
$\mathbf{C}-\mathbf{COO}$ stretching, $\mathbf{O}-\mathbf{CH}$ stretching, $\mathbf{O}-\mathbf{CO}$ stretching	1359
$\mathbf{C}-\mathbf{COO}$ stretching, $\mathbf{O}-\mathbf{CH}$ stretching, $\mathbf{CH_3}$ rocking, $\mathbf{CH}$ bending	1190–1180
$\mathbf{CH}$ bending or $\mathbf{O}-\mathbf{CH}$ stretching	1130
$\mathbf{C}-\mathbf{CH_3}$ stretching, $\mathbf{CH_3}$ rocking, or $\mathbf{CCO}$ bending	1080
$\mathbf{CH_3}$ rocking, $\mathbf{CH}$ bending, $\mathbf{C}-\mathbf{COO}$ stretching	1040–1060
$\mathbf{C}-\mathbf{COO}$ stretching, $\mathbf{C}-\mathbf{CH_3}$ stretching, $\mathbf{O}-\mathbf{CO}$ stretching	871
$\mathbf{C}-\mathbf{CH_3}$ stretching, skeletal $\mathbf{CCO}$ bending, $\mathbf{C}=\mathbf{O}$ bending	760

In *Figure 4-10* the spectra of the pure polymers and the drug, as well as for the binary polymer drug mixtures are depicted. For better visibility, the obtained spectra are arbitrarily aligned on the y-axis, sorted by the composition of the formulations and only the significant regions are shown (the whole spectra can be found in the Appendix).

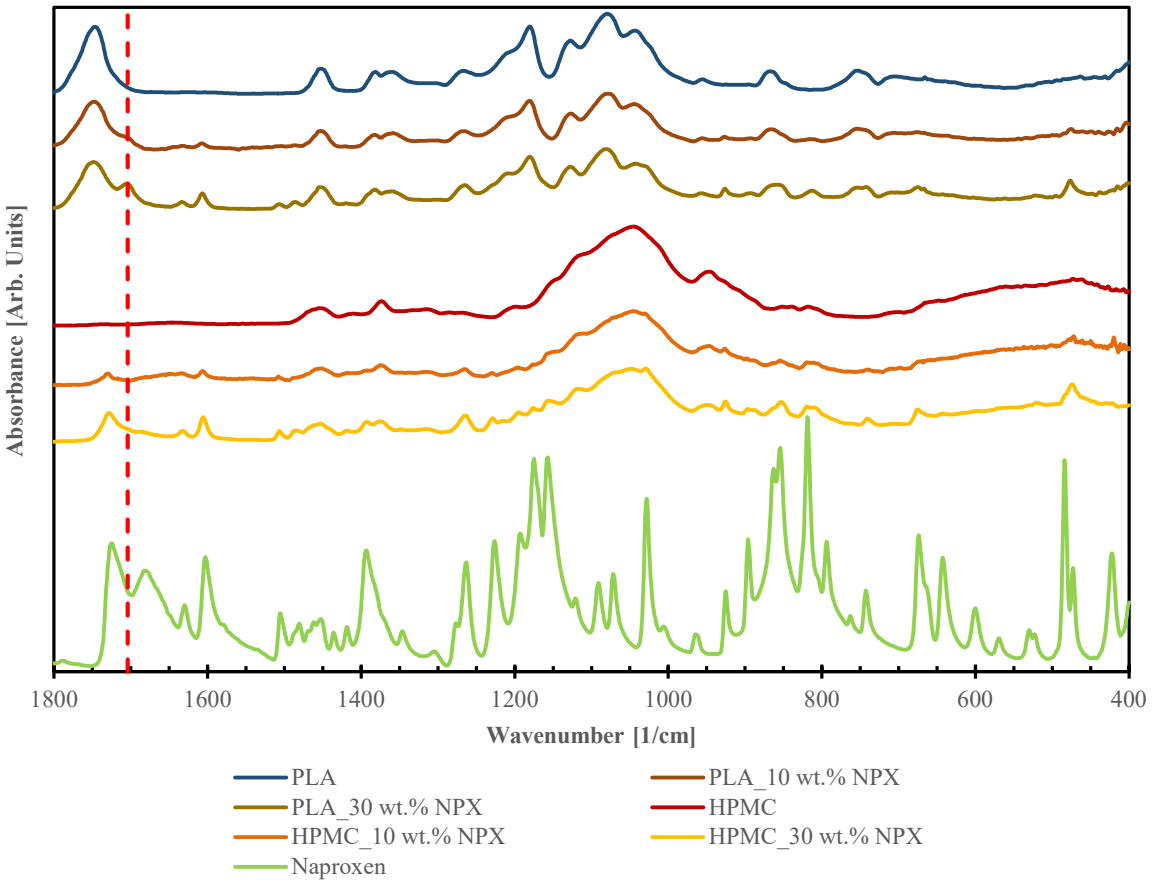

Figure 4-10: ATR-FTIR Spectra of the pure components as well as the influence of NPX on the mixture; the different spectra are arbitrarily aligned on the y-axis for better visualization

The spectra clearly show a decrease in intensity for the NPX peaks upon incorporation into the polymer matrices, possibly because of the changing state of order from crystalline to amorphous. For both polymers, there are no significant peak shifts visible except for the peak of C=O at 1720 cm^{-1} for pure NPX, shifting to 1704 cm^{-1} for the PLA and NPX blend. This shift can be attributed to H-bonds formed between the polymer and the API [52]. However, the same shift is not visible for the HPMC and NPX blend, suggesting a stronger interaction of PLA and NPX compared to HPMC. This contradicts the behaviour found during extruding where the viscosity of HPMC increased upon addition of NPX. Furthermore, the IR spectra indicate no degradation of the API, even though a black colour of the filaments was observed for the NPX-HPMC filaments.

Additionally, the same linear combination approach for the two polymers as for the WAXS was tested. The resulting spectra are an almost perfect match to the spectra obtained via measurement (cf. *Figure 4-11*). Therefore, the binary polymer mixtures show no shifts in their characteristic peaks, suggesting very limited interaction between the two polymers, which is consistent with the results obtained with DSC, indicating that the phases coexist in the matrix and are indeed phase separated.

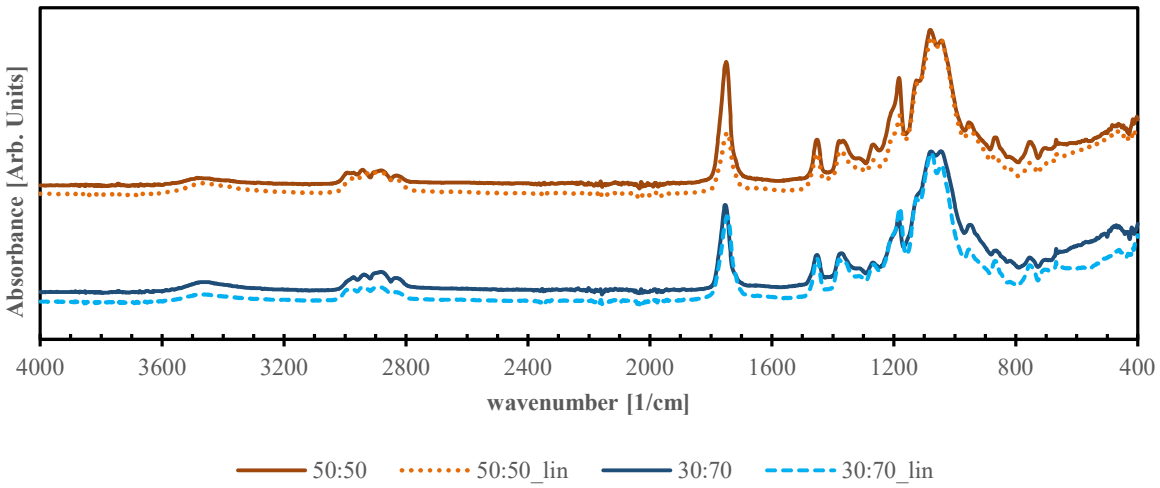

Figure 4-11: Linear combination of the pure component data compared to measured spectra of the polymer ratios 50:50 and 30:70

The following normalized IR diagrams (cf. *Figure 4-12*) show the absorption spectra of the different polymer mixtures, as well as the ternary formulations. The previously mentioned shift due to H-bonds formed between PLA and NPX can also be seen in the ternary formulations with a high PLA content. For the formulations with a ratio of 30:70, however, this shift is less pronounced. Considering the spectra of the pure components, it is obvious that several characteristic peaks overlap, which is why possible peak shifts are even harder to detect. Further insight into the interactions of the components might be obtained by a deconvolution of the peaks [52], which was not within the scope of this thesis.

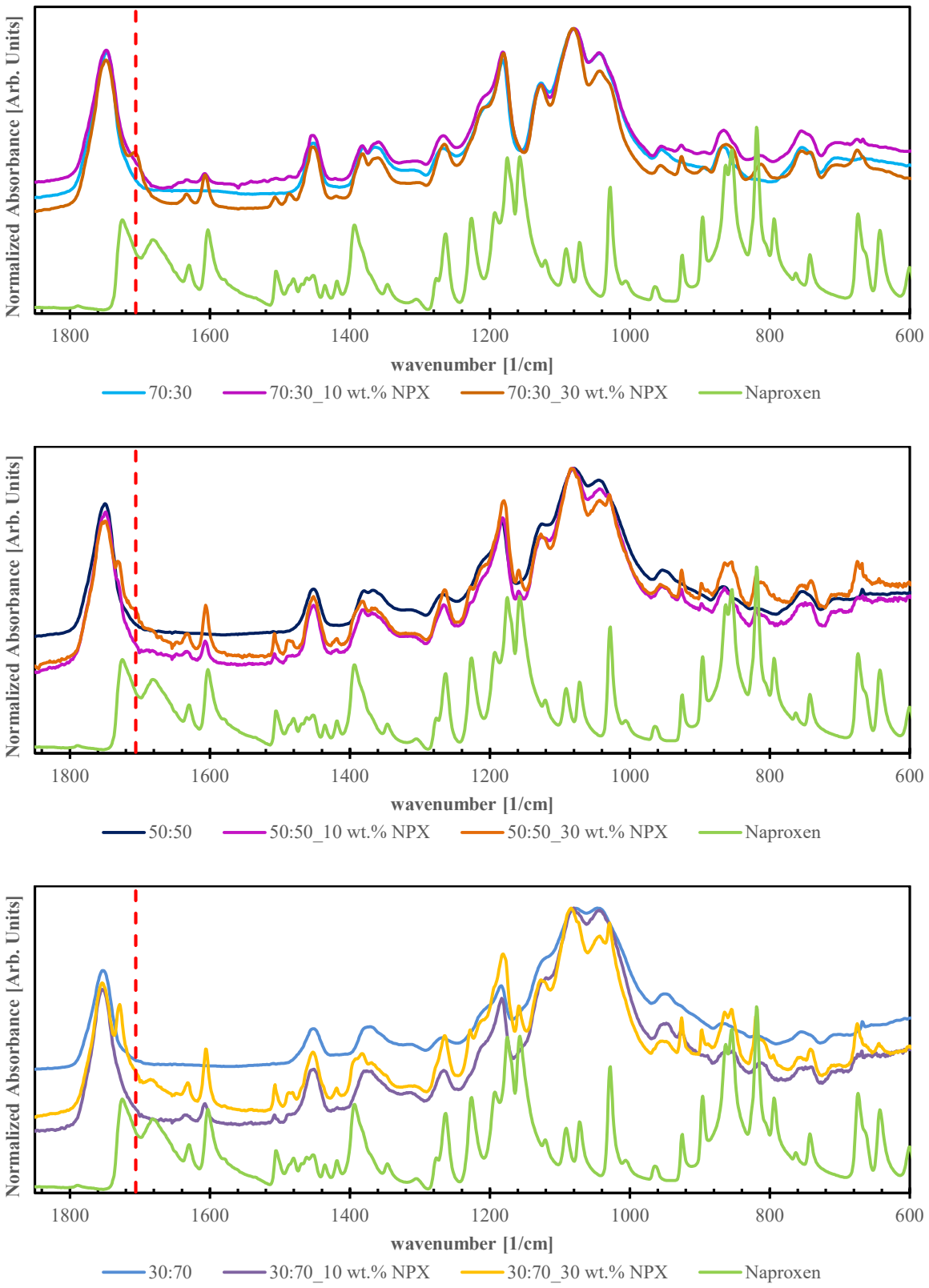

Figure 4-12: Normalized ATR-FTIR spectra for the different polymer ratios and drug contents; the pure NPX is not normalized and arbitrarily aligned on the y-axis for better visualization. The normalization was made relative to the highest peak within the depicted range for each formulation, respectively [52].

4.6 PHASE BEHAVIOUR BEFORE RELEASE

To investigate the structural arrangement and the phase behaviour after extrusion, Raman mapping was utilized. In order to assign the false colour scheme of the map, the pure components were analysed in the form of filaments (PLA and HPMC) and powder (NPX), cf. *Figure 4-13*.

The results indicate a significant challenge with Raman mapping, where characteristic peaks for the individual materials need to be found to allocate the measured spectra to the different components. Individual characteristic peaks can be seen for PLA and NPX as indicated by the peaks in the shaded areas (red and green), but not for HPMC (blue), since all characteristic HPMC peaks are overlapping with peaks of the other two components, meaning they cannot be distinguished in the resulting spectra. However, HPMC exhibited a very high luminescence in contrast to PLA and NPX and therefore the region without any contributions from the other two components is used to identify HPMC in the sample. The allocation for the map in the software is done based on the peak areas.

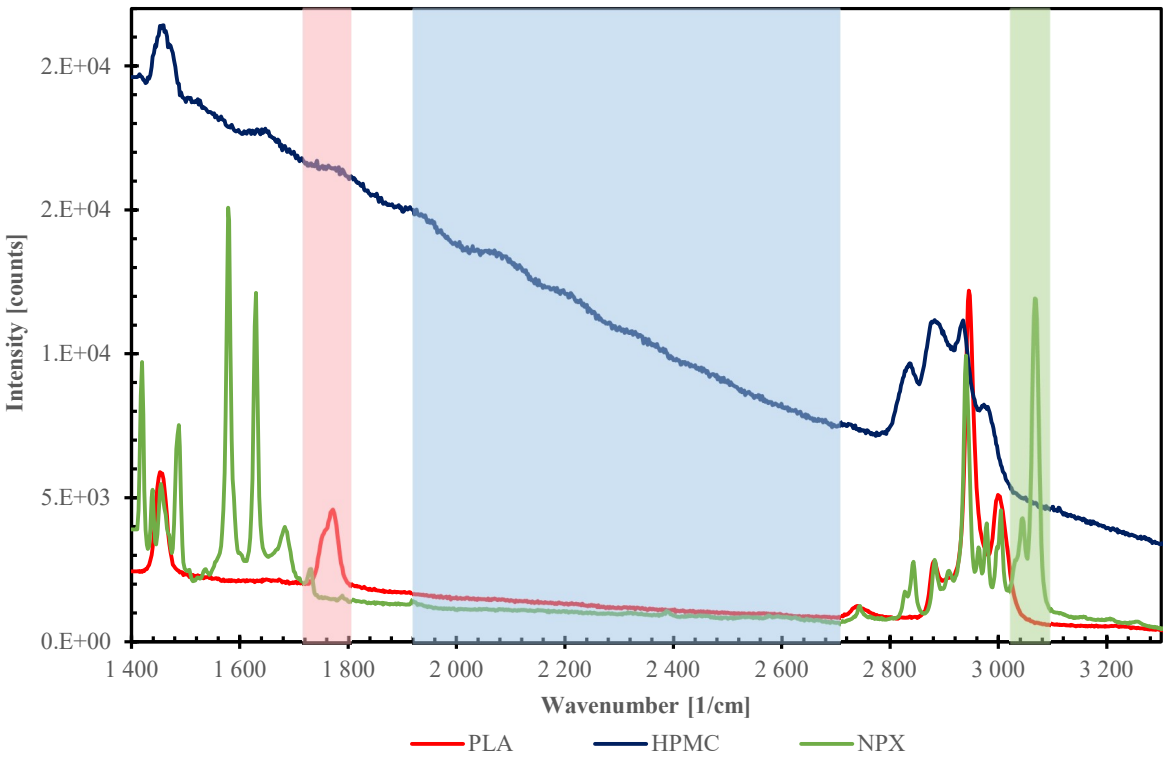

Figure 4-13: Raman spectra of the pure components obtained with a 633 nm laser (red), with the transparent areas indicating the areas used for the peak assignment

To investigate the scale of the structural characteristics, in the first run a 75x25 *µm* map is measured with an acquisition time of 6 *sec* of the formulation of 30:70_ 30 wt.% NPX (cf. *Figure 4-14*).

The individual maps for the present components in the sample can be seen in the pictures (a) for PLA, (b) for NPX and (c) for HPMC. A brighter colour, and therefore higher intensity, indicates a higher concentration of the respective material. With these three maps an overlay is created, with the individual measurement points displayed as pixels (d) and applied smoothing of the pixels (f). The map is obtained by normalizing the peak intensities to the highest peak of the respective components and subsequently comparing the three materials. The colour displayed for each pixel has the highest normalized intensity at this point and therefore is the predominant one, but this component is not the only component present at this point. Picture (e) shows the position of the mapped area on the sample's surface under the Raman microscope.

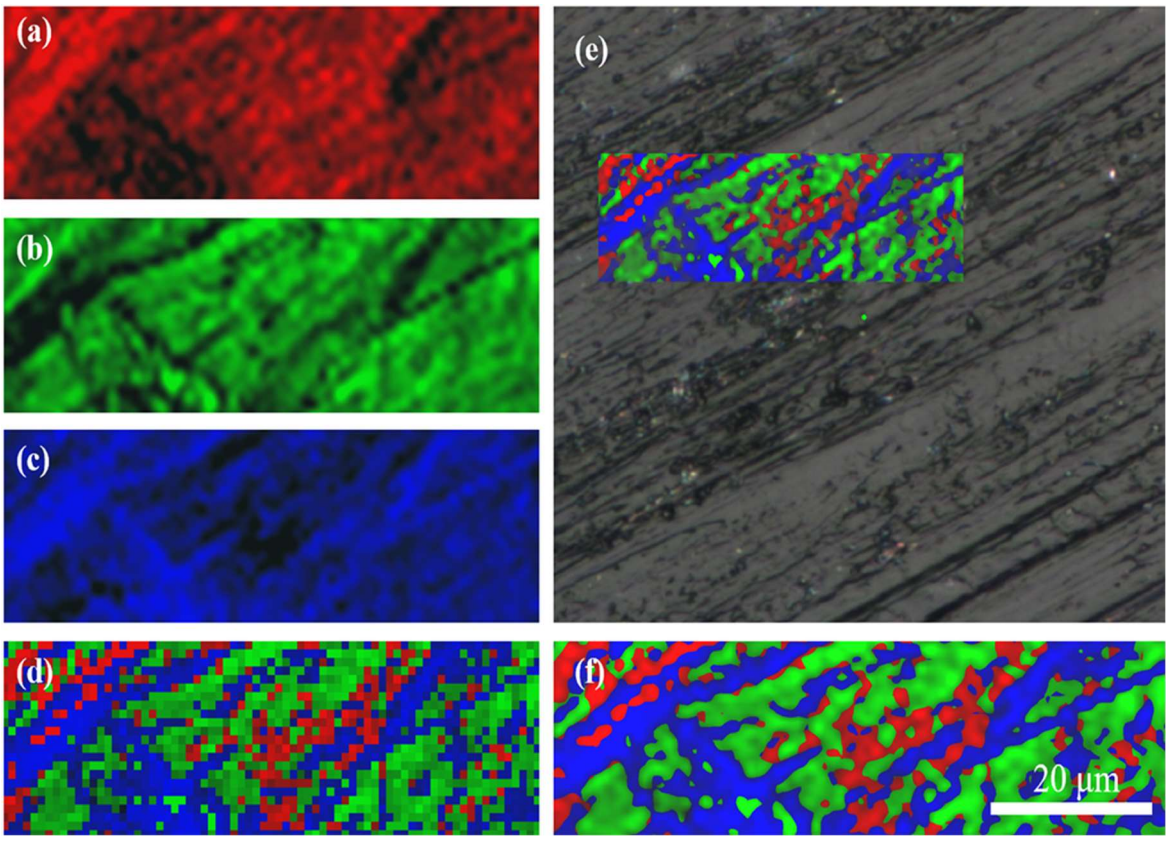

Figure 4-14: Results of the Raman mapping for the formulation 30:70_30 wt.% NPX with the individual maps of PLA (a), NPX (b) and HPMC (c); (d) resulting overlay of the three maps depicted without smoothing; (e) position of the map on the surface of the cross-section of the sample shown under the microscope; (f) final map of the sample with smoothed regions

Furthermore, the percentage of the substances becomes clear, namely that the formulation contains more NPX than PLA, as well as the fact that the API seems to be embedded in the PLA phase as well as the HPMC phase. An inhomogeneous distribution of the colours over the map indicates that phase separation upon extrusion of the mixtures occurred.

Similar to the previous sample, two other formulations are investigated (cf. *Figure 4-15*). Since the mapping of the previous sample took over 15 *h*, the acquisition time is reduced to 4 *sec* for the other two samples to be able to map a larger area with the same resolution. The measurement then lasted approximately 6 *h* for both samples respectively.

The obtained maps for the polymer ratios 70:30 (left picture) and 50:50 (right picture), both with 10 wt.% NPX content show the same structural arrangement as the filament with higher drug content. The left map clearly indicates a high PLA percentage whereas the two polymers are evenly present in the 50:50 formulation as expected. Furthermore, there are clear drug-rich domains within both samples.

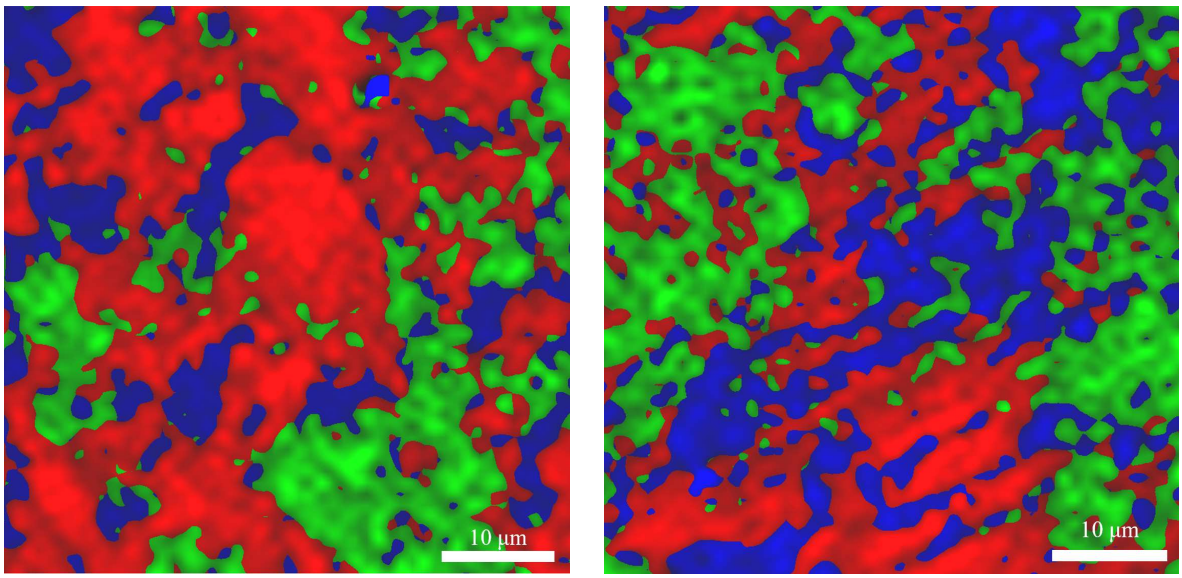

Figure 4-15: Overlayed Raman maps for the formulations 70:30_10 wt.% NPX (left) and 50:50_10 wt.% NPX (right)

These results demonstrate that Raman mapping can provide valuable insight into the phase behaviour of the polymers and confirms the already presumed phase separation of the two polymers. Surprisingly, the drug-rich domains are quite large for the latter two samples, considering a content of only 10 wt.% API. That could be either attributed to a very high intensity of the drug compared to the polymers and therefore a possible visual illusion because of the colour assignment, or because more drug is present in the middle of the filaments, where the measurements were performed.

4.7 QUANTITATIVE ANALYSIS: IN VITRO STUDIES

To quantitatively determine the effect of the previously mentioned phenomena the drug release rates of the filaments are tested in vitro. The experiments are used to describe the influence of polymer ratio,

surface area and drug content by means of determining the release speed, release kinetics and the extend of polymer swelling.

4.7.1 Necessary Calculations and Properties of the Filaments

To calculate the amount of drug released over time from the UV-Vis analysis, a calibration curve of NPX in phosphate buffer is generated (cf. *Figure 7-1*, Appendix). The determined relation between the absorption A and concentration c_t of the API can be seen in *Equation 4-2*.

$$A = 307.73 \cdot c_t \left[\frac{mg}{ml}\right] + 0.0564 \qquad 4\text{-}2$$

Since the experiments are carried out over long periods of time, losses due to evaporation need to be considered. Additionally, the amount withdrawn with each sampling step needs to be taken into consideration to accurately calculate the mass m_t of NPX for each sampling point from the concentration c_t in the release baths. The evaporation loss V_{loss} in *ml/h* was determined by measuring the volume of the remaining phosphate buffer after completing the experiment and dividing the lost volume by the number of hours the experiment lasted in total.

Additionally, the mass of drug removed via each sampling step was calculated with a cumulative sum over the volume of all samples removed at each point *t,* the concentration c_{i-1} in the bath one sample before point *t* and V_s, the volume of the sample (cf. *Equation 4-3*).

$$m_t[mg] = c_t\left[\frac{g}{ml}\right] \cdot \left(900[ml] - \left(V_{loss}\left[\frac{ml}{h}\right] \cdot t\,[h]\right)\right) + \sum_{i=2}^{t} c_{i-1}\left[\frac{mg}{ml}\right] \cdot V_S\,[ml] \qquad 4\text{-}3$$

To compare the results of different pieces, the mass m_t must be normalized. Therefore, the mass at each point was divided by the expected amount of drug m_0 within the filament, calculated via the total mass of the filament piece (cf. *Equation 4-4*).

$$release\ [\%] = \frac{m_t}{m_0} \cdot 100 \qquad 4\text{-}4$$

The dimensions of the used filament pieces as well as the mass of the pieces and consequently the expected mass of NPX within the pieces (calculated based on wt.%) are shown in *Table 4-8.*

Table 4-8: Average properties (n=3) of the filament pieces used in the release studies for each formulation

Property	30:70		50:50		70:30	
	10 wt.%	30 wt.%	10 wt.%	30 wt.%	10 wt.%	30 wt.%
Mass [mg]	54.77	15.30	54.87	15.77	49.43	19.36
Mass NPX [mg]	5.48	4.59	5.49	4.73	4.94	5.81
Diameter [mm]	1.79	1.86	1.69	1.74	1.78	1.87
Length [mm]	18.88	4.52	21.49	5.52	15.88	5.77
Surface Area [mm²]	108.58	29.06	116.11	32.64	93.52	39.43

To test the homogeneity and have statistically representative values, the release studies are carried out in triplicate for each formulation. The depicted dimensions are the average of the three filament pieces used for each formulation. The diameter for each filament was determined with a micrometer, and the length is measured using a calliper.

The possibility to influence the results by reaching the saturation concentration is reduced by using smaller pieces for the samples containing 30 wt.% than for the 10 wt.% samples. The solubility limit of NPX in phosphate buffer with a pH-value of 6.8 is in the range of 0.2 *mg/ml* [54]. Therefore, the size is chosen based on the final API mass, which consequently leads to a much lower outer surface area for the samples with higher drug content. Since a 30 wt.% piece in the same size as the 10 wt.% sample leads to a concentration closer to the saturation limit, the pieces had to be smaller. Additionally, using smaller pieces avoids diluting the samples to obtain an absorbance within the validity of the Lambert-Beer's Law for the UV-Vis analysis, hence excluding another factor influencing the results.

Nevertheless, a possible influence of reaching the saturation limit of the drug during the release studies was tested for two samples by removing 250 *ml* of the release medium (out of 900 *ml*) after a release of 90 % and replacing it with fresh phosphate buffer. No significant change in release speed was observed afterwards. This proves that the release rate is not influenced by reaching the saturation limit.

To better compare the results, the release rate is also normalized with the surface area according to *Equation 4-5,* since the available surface area has a significant influence on the drug release. The normalization is only done for the first 8 *h* of the experiments. In those hours, all samples showed time-independent release behaviour (a straight regression line can be obtained), where k is the slope of the concentration regression line ($\mu g/ml$ over h), not taking the origin of the line into account, V is the total volume of the phosphate buffer (900 *ml*), and S is the outer surface area of the pieces in mm^2.

Equation 4-6 additionally takes the weight fraction *w* of NPX in the respective samples into account (with the assumption that the densities of the components are similar, this can also be seen as the volume fraction).

$$A\left[\frac{\mu g}{mm^2 \cdot h}\right] = \frac{k \cdot V}{S} \qquad 4\text{-}5$$

$$A\left[\frac{\mu g}{mm^2 \cdot h}\right] = \frac{k \cdot V}{S \cdot w} \qquad 4\text{-}6$$

The results of the dissolution studies, the obtained release curves, and a kinetic analysis of the release mechanisms are depicted in the following subchapter.

4.7.2 Influence of Polymer Ratio

To investigate the influence of polymer phase separation for extended drug release, three different polymer ratios 70:70, 50:50 and 30:70 and two different drug contents were investigated in the release studies. Additionally, pure PLA with NPX was tested as a reference. Release studies of samples containing HPMC and NPX were chosen not to be performed, since the produced filaments show a significant influence of fouling (*cf. Chapter 4.2*).

In *Figure 4-16* the results for filaments with 10 and 30 wt.% NPX are depicted. The drug release rate in a solid dispersion is controlled by the polymer release rate for low drug content [16], [44]. Since HPMC is a hydrophilic polymer and therefore far more water-soluble, the release rate was significantly faster with increasing HMPC percentage. The apparent faster release for the 10 wt.% samples compared to the 30 wt.% samples will be discussed in detail in *Chapter 4.7.3*, since these release curves were not normalized to the surface area.

The standard deviation was generally higher for the filaments with higher drug loading, however, this is assumed to be only because the 10 wt.% pieces were larger than the 30 wt.% samples.

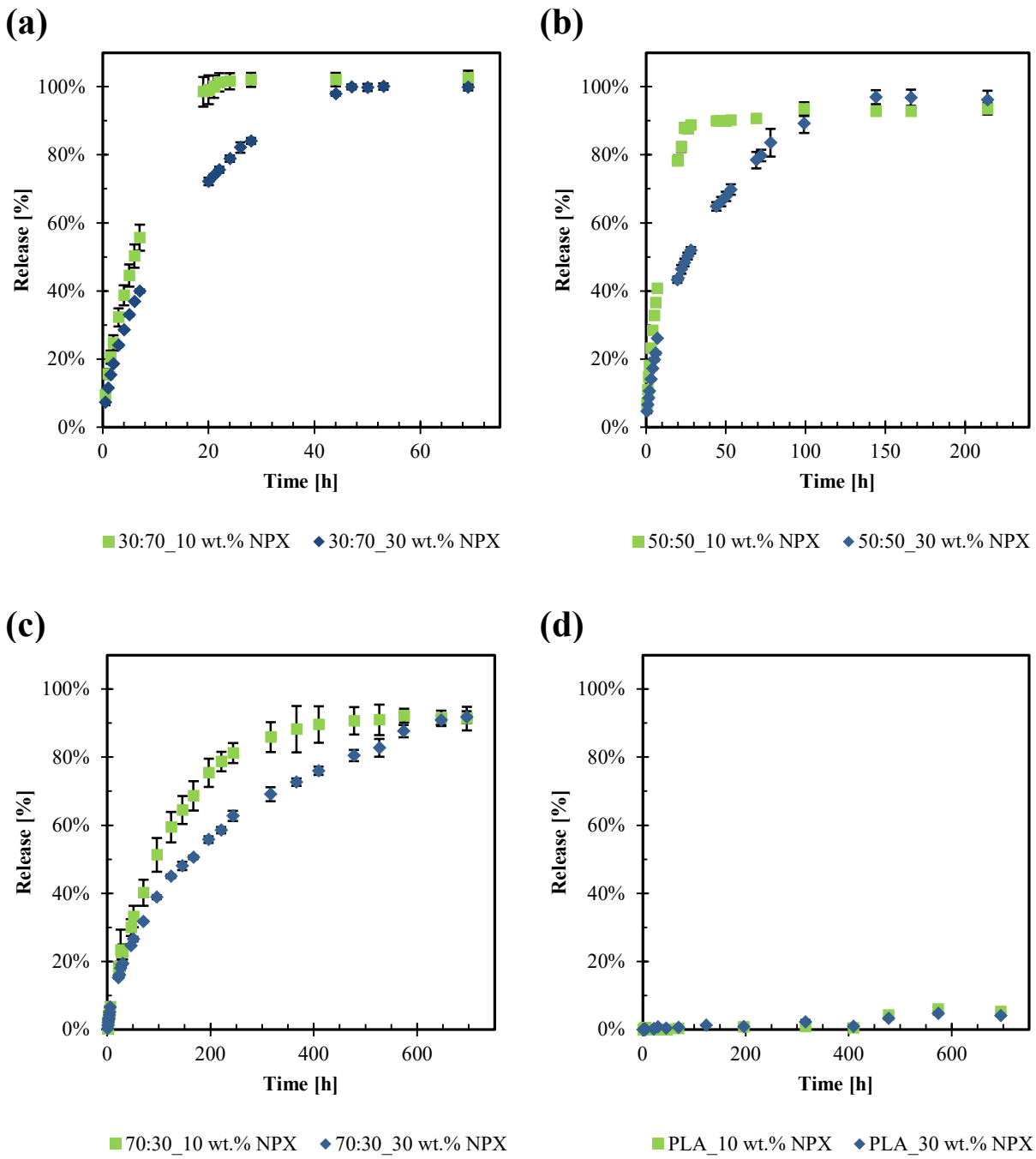

Figure 4-16: Release curves for the investigated formulations (a) 30:70; (b) 50:50; (b) 70:30; (d) PLA. Error bars represent the standard deviation for the experiment carried out in triplet (n = 3), and may be smaller than the symbols for some points

Overall, the standard deviation of all experiments is very low, especially for high HPMC content, suggesting homogenous distribution of the drug over the length of the extruded filament. For the 70:30 samples (c), the standard deviation is slightly larger, although only by a few percent and furthermore very consistent, suggesting a small difference between the pieces but a smooth release for the individual samples.

The experiments with PLA (d) show that there was virtually no release for over 400 *h* and the concentration was on the verge of the detection limit of the UV-Vis device, which leads to a high standard deviation compared to the other experiments. After 700 *h* the release was approx. 5 % for both the 10 and 30 wt.% samples. This shows that formulations with pure PLA are not relevant for oral administration.

Furthermore, as previously stated, filaments with only HPMC could not be used for release studies due to fouling during HME and possible degradation of the API. However, a blend of the two polymers leads to promising release results. A ratio of 70:30 shows a uniform release curve with full release after 550 *h* for 10 wt.% and 700 *h* for 30 wt.% drug content. Considering the convergence of the 70:30 release curve, only about 90 % of the drug were released for both drug contents. The DSC and Raman results indicate that the drug was distributed within the PLA phase as well as the HPMC phase, but the hydrophilic HPMC is determining the release of NPX, because PLA is only slightly soluble in the phosphate buffer, and therefore the drug cannot leak out. However, the overall HPMC content in this formulation is only 27 wt.%, which indicates that the HPMC is dispersed in a continuous PLA phase, and the release behaviour therefore can be explained by the percolation theory [55]. This suggests that the low HPMC volume might be too small to form "percolating channels" within the filament and the PLA matrix therefore inhibits the water penetration. Nonetheless, the release curve shows that the HPMC content is high enough to be able to release 90 % of the API, and only few regions cannot be reached by the water.

The formulation with a 50:50 polymer ratio (b) additionally shows only 90 % release for the 10 wt.% sample, after approx. 75 *h*, however for higher drug content, full release is reached after 140 *h*. The reason for reaching a full release with 30 wt.% but not 10 wt.% might be explained by the ratio of water-soluble to water-insoluble volume. HPMC and NPX were allocated to the water-soluble volume and PLA to the water-insoluble volume. This allocation illustrates that for higher drug content the water-soluble volume increases, and percolation can be achieved more easily. For the highest HPMC content with a polymer ratio of 30:70 (a) full release is reached after approx. 20 *h* for the 10 wt.% samples and 40 *h* for the 30 wt.% samples with the full release indicating that all of the drug could be dissolved because of the high HPMC content and consequently a lack of percolation limitation.

In general, the dissolution studies for polymer ratios of 50:50 and 30:70 show a minor burst release of API in the beginning of the experiments, probably because of drug located close to the surface area of the filaments. Furthermore, it can be observed that the release rate is much faster for the first 50 % of

API released and slows down afterwards. This behaviour is even more pronounced for higher PLA content.

For better comparison, *Figure 4-17* depicts the first 72 *h* for all the experiments containing a polymer mixture (since it is not practical to show the entire experiments in one diagram). The combined plot reinforces the different release speeds for the three polymer ratios. Additionally, the decrease in the release rate over time can be seen more pronounced. The obtained release curves show a strong influence of the polymer ratio on the release, and that a considerable variation of release rates can be obtained with different formulations, therefore presenting possible applications in oral (fast release) and transdermal administration (slow release).

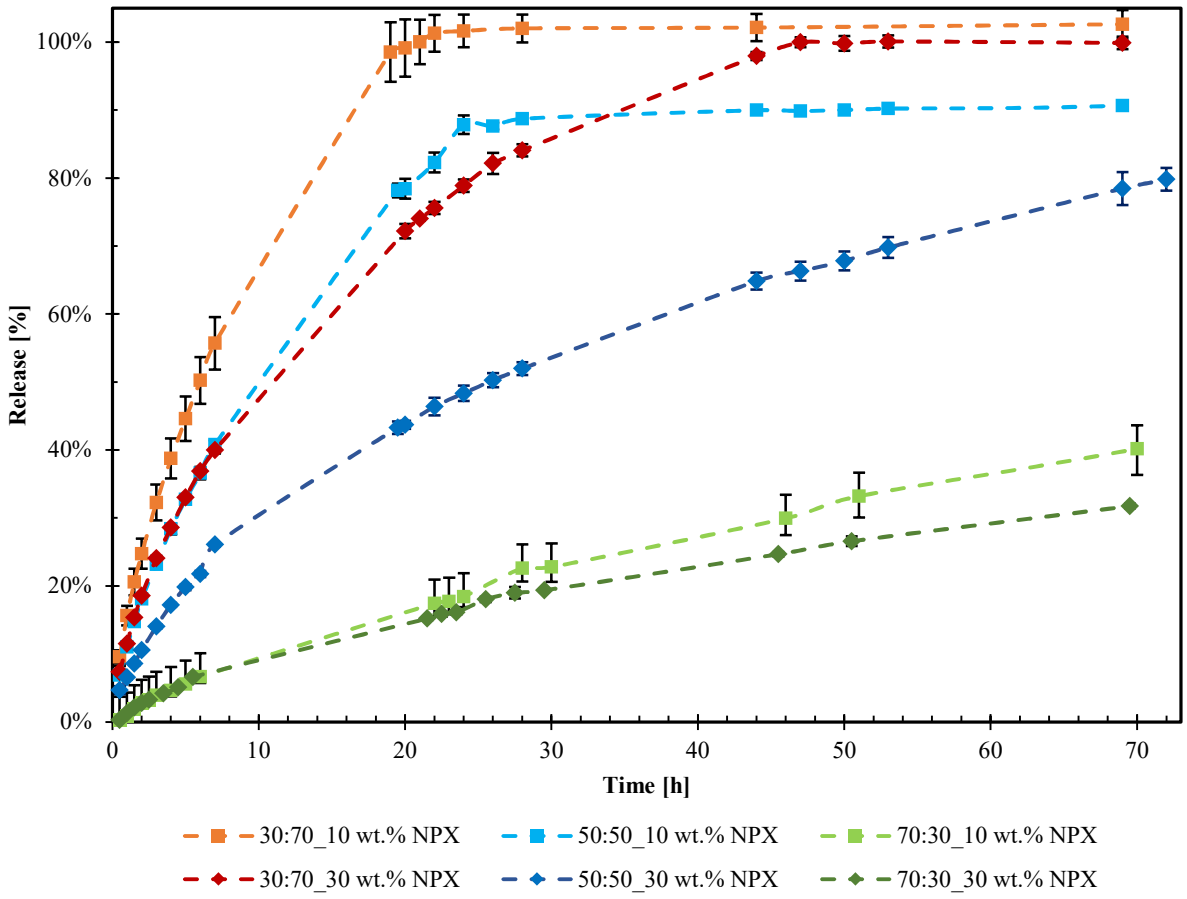

Figure 4-17: Comparison of the NPX release for the different polymer mixtures over the first 72 hours. Error bars represent the standard deviations for the experiments carried out in triplet (n = 3), and may be smaller than the symbols for some points

The previously mentioned slower release can be visualized more clearly by plotting the release over the square root of time (cf. *Figure 4-18*). This representation of the data illustrates the effect of the PLA matrix on the release rate of the drug because the release slows down over time. This indicates that at a specific point, there is only NPX either within the PLA phase or the HPMC/NPX mixture is encapsulated

in a PLA area, leading to a reduction in release speed and the convergence of the released mass to 90 %. Overall, there seems to be a constant release speed for the first 60–80 % of released mass, depending on the formulation, indicated by an approximately linear increase. Afterwards, the slope changes and a reduction in release speed is visible.

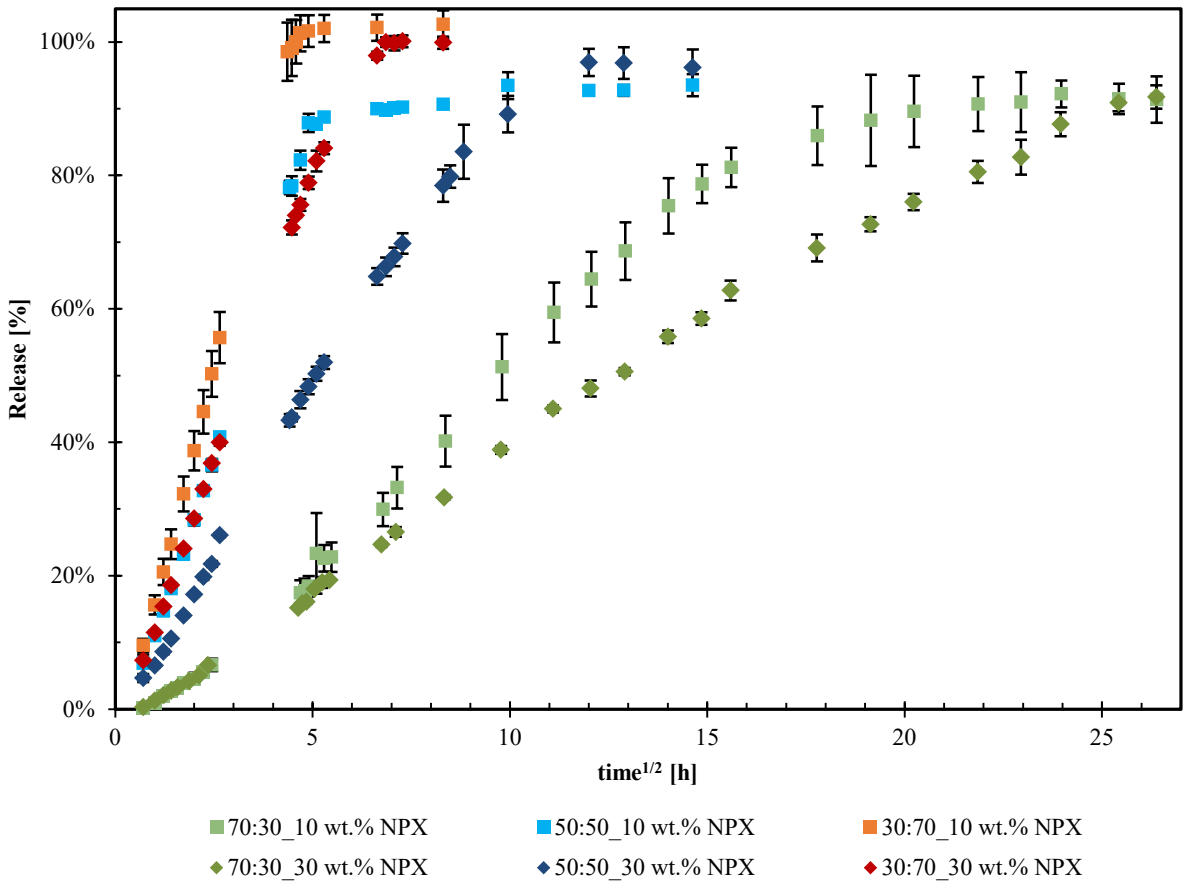

Figure 4-18: Percentage release plotted over the square root of time to show the influence of the PLA matrix. Error bars represent the standard deviations for the experiments carried out in triplet (n = 3), and may be smaller than the symbols for some points

Here it should be mentioned that the phenomena of an incomplete release, and a possible percolation threshold, are not visible if the experimental value of full release is used for the normalization and not the estimated amount of NPX. Nonetheless, it should be ensured during extrusion that the whole drug amount can be embedded within the filament to avoid erroneous results.

4.7.3 Influence of Surface Area and Drug Content

To test the influence of different drug contents, filament pieces with 10 and 30 wt.% NPX were tested. As mentioned before, a higher drug content provides challenges for the extrusion process. Dissolution studies, however, showed a smooth release curve with a low standard deviation. The release curves depicted in *Chapter 4.7.2* suggest that the release rate was decreasing with increasing drug content. To

investigate if that only applies due to a consequently reduced contact area for the dissolution medium because of a lower surface area, the dissolution rate was normalized with the surface area and the drug content. This normalization is only done for the first 8 *h* of every experiment since within this time period a linear regression of the release data is possible (cf. *Equation 4-5* and *4-6*). In *Figure 4-19* the results of this normalization are shown. The left plot shows the normalization with the surface area, not taking the drug content into account.

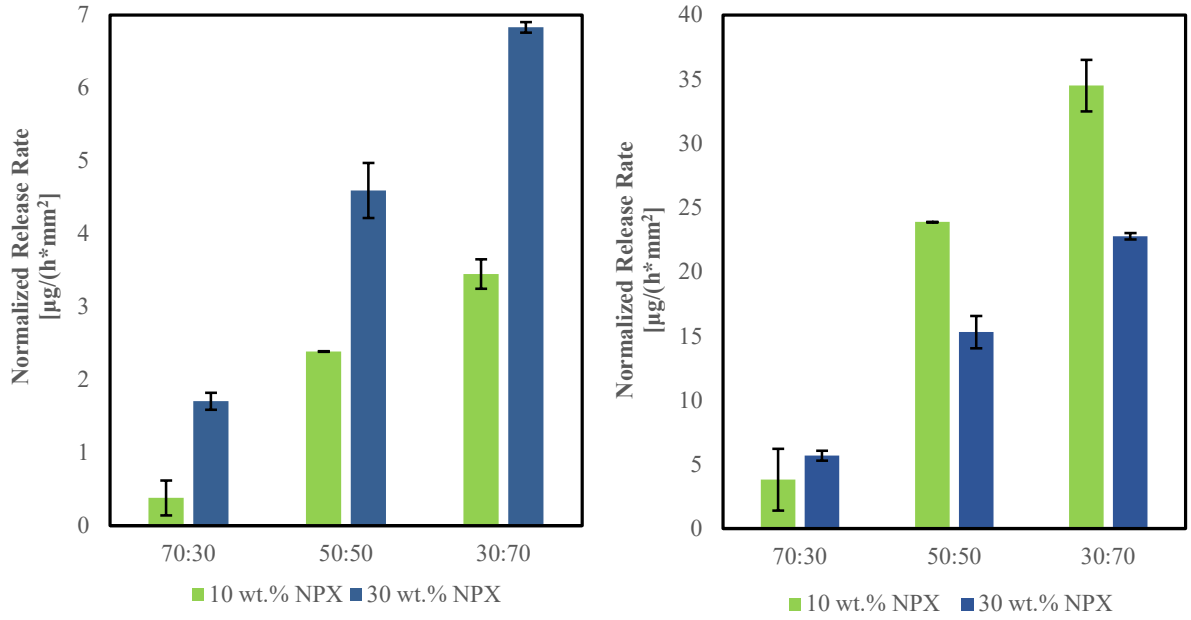

Figure 4-19: Normalization of the release rate over the first 8 hours of the experiments; only normalized with the surface area (left); normalization includes the weight percentage of the drug (right). Error bars represent the standard deviations of the three filament pieces used for each formulation (n=3)

First, this normalization strengthens the conclusion already discussed before, that the release rate increases significantly with increasing HPMC content. Second, if the weight fraction of NPX is not considered, it seems that the release rate is significantly faster for higher drug content. Additionally, the standard deviation was not always larger for lower drug content than for higher drug content, as the non-normalized release curves would suggest and the lower standard deviation for higher drug content in the release curves occurs only because of a lower surface area.

Considering the weight fraction of API in combination with the surface area (right plot), the release speed is indeed slower for higher drug content. This behaviour can be explained by the fact that for ASDs the release speed of the drug is predominantly controlled by the release speed of a hydrophilic polymer (HPMC), since the release rate of the polymer is several magnitudes higher than the release rate of the pure amorphous drug [16]. For higher drug contents, there is considerably less HPMC present in the formulation, which leads to a decrease in the release rate. Furthermore, this influence of the drug

content is more significant for increasing HPMC content since the formulation with 70 % PLA shows almost no influence of the drug content on the release rate.

Overall, it can be concluded that the outer surface area of the filament as well as the drug content have a significant influence on the release rate of NPX.

4.7.4 Polymer Swelling

The validity of most kinetic models to describe the release behaviour of drugs depends on the extension of swelling of the polymer systems. For example, the simple Korsmeyer-Peppas model is still applicable for slightly swelling systems like formulations with HPMC, but only if the swelling of the system is not more than 25 % of its original volume [56].

In *Figure 4-20* the filament pieces for two formulations containing 30 wt.% NPX are depicted before (left sample) and after (right sample) release. It becomes clear that there was significant swelling of the filament pieces during release. The pictures indicate that the swelling is more pronounced for HPMC than for PLA because the increase is visibly larger for the 30:70 polymer ratio than for the 50:50 ratio.

Additionally, a colour change can be observed for the filaments. A higher porosity leads to higher light reflection, and consequently the sample appears to be white.

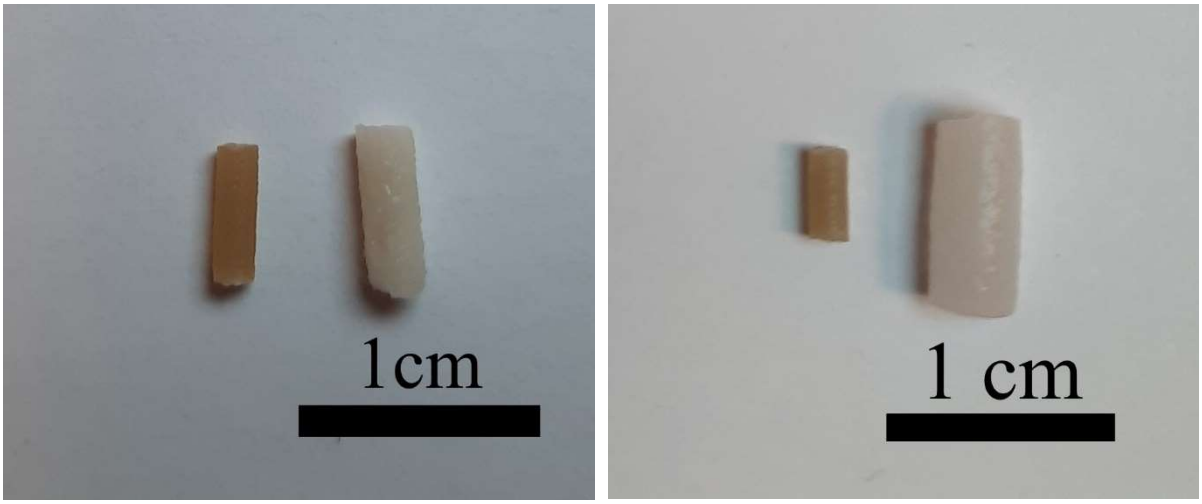

Figure 4-20: Left image: 50:50_30 wt.% NPX, before release (left) and after release (right); right image: 30:70_30wt.% NPX before release (left) and after release (right)

For a quantitative determination of the swelling, the diameter and length of the pieces were measured with a micrometer and a calliper, respectively, before and after release. The increase of the filament diameter during release is shown in *Figure 4-21* (left diagram).

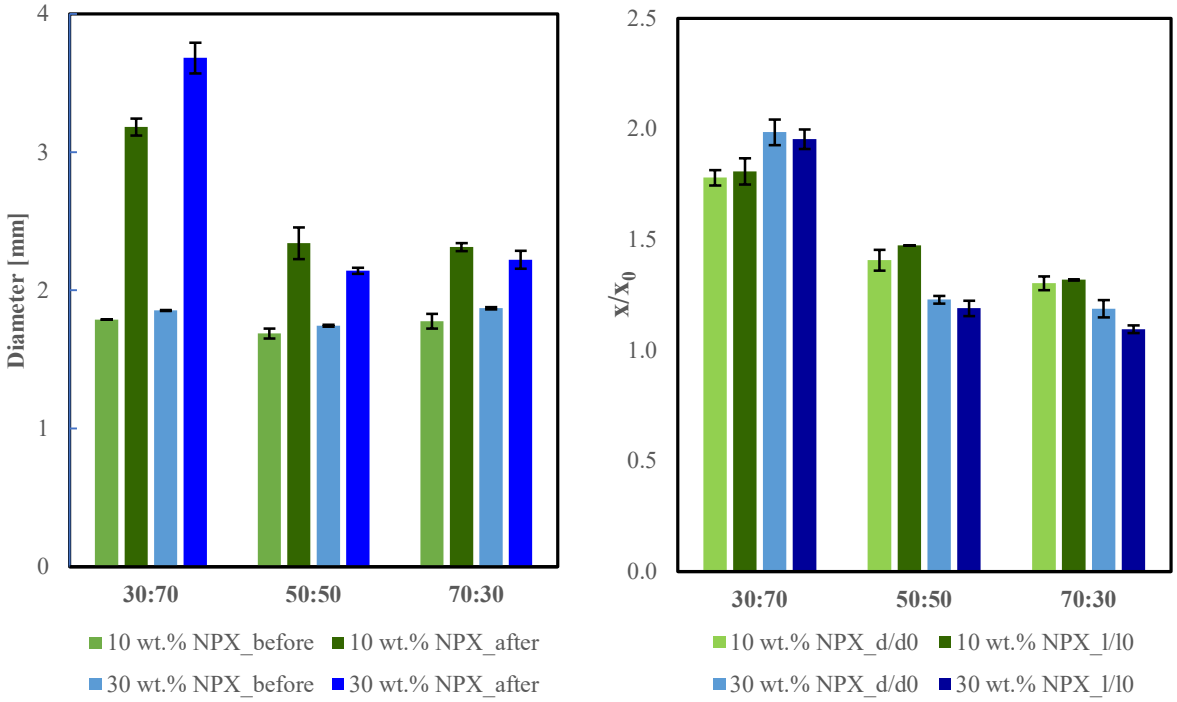

Figure 4-21:Comparison of the filament diameter before and after release (left); diameter and length ratio before and after release (right). Error bars represent the standard deviations of the three filament pieces used for each formulation (n=3)

To determine if there is an orientation of the polymer chains, which would mean either the diameter or the length displays a stronger increase, the ratio of the dimensions after release and before release x/x_0, where x is either the diameter or the length of the filament, were additionally calculated (right diagram). The error bars in the pictures represent the standard deviation of the three pieces used in the dissolution studies for each formulation.

The diagram strengthens the observations from the filament pieces shown in the previous pictures. However, it should be mentioned that it is difficult to measure the dimensions after release because the pieces are in a soft rubber-like state and can be deformed easily. This means that the measurements are not highly accurate and therefore leading to a much higher standard deviation compared to the measurements prior to the release. Both calculations show a significant increase during the release for every formulation. For the polymer ratios 50:50 and 70:30 the relative increase is larger for the 10 wt.% samples. For the 30:70 ratio the opposite is the case.

Calculations show that the diameter increases by 78 % for the 10 wt.% sample and 98 % for the 30 wt.% sample for the 30:70 polymer ratio, however only by 30 % for the 10 wt.% sample and 19 % for the 30 wt.% samples for the 70:30 polymer ratio. For the 50:50 samples the results are as expected in-between the values for 30:70 and 70:30, with 39 % for the 10 wt.% sample and 23 % for the 30 wt.% sample.

Furthermore, it can be observed that the polymer chains are not clearly orientated inside the matrix since the diameter and length ratios are similar for all the formations. This suggests that the polymers are not aligned in some specific way during the extrusion process. In general, these results show that the release behaviour is clearly influenced by the swelling of HPMC upon contact with water.

4.7.5 Release Kinetics

An attempt was made to fit the release data up to a release of ~ 60 % to the Korsmeyer-Peppas model using the Excel solver to characterise the release mechanism. The used model is shown in *Equation 4-7*, where M_t is the mass of NPX released until time t and M_∞ is the theoretical mass of NPX in the sample. The variables k, the release constant and n, the release exponent, are the fitted model parameters [56], [57].

$$\frac{M_t}{M_\infty} = k \cdot t^n \qquad 4\text{-}7$$

In general, this model is also applicable for swelling polymeric systems if the swelling is less than 25 % (water content based on the volume) or the swelling ratio is less than 1.33 (related to the weight increase) [56]. Since the swelling of the filaments is significant this model might not be suitable to describe this system, especially for high HPMC content. Nonetheless, this model is frequently used due to its simplicity to estimate release mechanisms for systems, even though the criteria stated by Korsmeyer and Peppas is not fulfilled.

Although aware of the limited applicability of this model for the present system, it was decided to include the results of the model anyhow. Surprisingly, the model's finding corresponds well with the other observations already made and allows a clarification, or at least an indication, of the possible underlying release mechanism. *Table 4-9* summarizes the results for the kinetic constant k, the diffusional exponent n, and the coefficient of determination R^2.

In literature, the limits for release from cylindrical systems the n-value for Fickian diffusion should be 0.45, whereas n-values in the range of 0.45 – 0.89 represents anomalous transport and erosion controlled systems [56]. The coefficient of determination for each fit indicated an accurate fit and smooth release data. The diffusional exponent n is between 0.45 and 0.89 for all investigated systems indicating anomalous transport, furthermore, n is lower for the systems with higher drug content. This supports that the penetration and diffusion of water inside the matrix is easier for formulations with higher drug content.

Table 4-9: Results of the fit for the Korsmeyer-Peppas model

Formulation	k	n	R^2
30:70_10 wt.% NPX	0.16	0.65	0.9999
50:50_10 wt.% NPX	0.12	0.64	0.9998
70:30_10 wt.% NPX	0.02	0.69	0.9969
30:70_30 wt.% NPX	0.13	0.59	0.9986
50:50_30 wt.% NPX	0.08	0.56	0.9969
70:30_30 wt.% NPX	0.03	0.56	0.9982

However, it is not reasonable that the diffusional exponent is higher for 10 wt% NPX and the 70:30 polymer mixture. This discrepancy might be explained by the fact, that the other filaments exhibit the most significant swelling and therefore the model might give erroneous results. Furthermore, the kinetic constant k decreases with increasing PLA content and these results agree with the previously observed trend seen in *Figure 4-19*.

4.8 PHASE BEHAVIOUR AFTER RELEASE

Filament pieces are analysed after release to characterise the remaining polymer matrix and compared with Raman images taken before being exposed to water, to determine if the phase separation was induced by water or already occurs during the HME process.

To show the influence of the drug content and the polymer ratio on the phase separation, the surface area and the cross-section of the filaments were analysed with SEM. The structure of the surface area was analysed for the 70:30 formulations (cf. *Figure 4-22*)

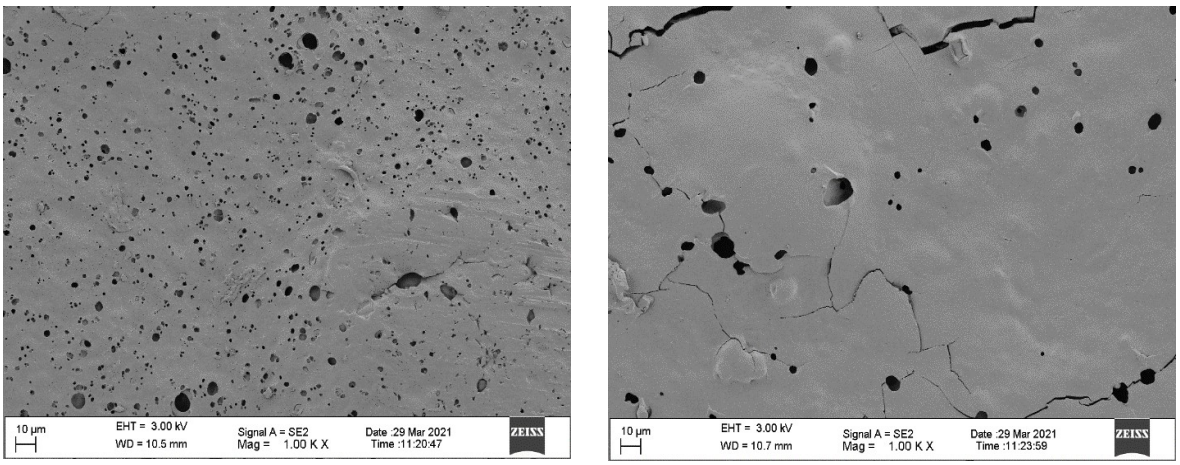

Figure 4-22: SEM images of the filament surface at 1k magnification; left Image: 70:30_10 wt.% NPX; right Image: 70:30_30 wt.% NPX

By comparing the two formulations with different amounts of drug it becomes clear that the sample with only 10 wt.% drug (left) shows a much larger number of pores in the remaining PLA matrix than the sample containing 30 wt.% NPX (right). As previously mentioned, this can be explained by a lower drug content leading to a higher absolute value of HPMC mass within the filaments, and thus the hydrophilic HPMC can create more pores for the samples containing 10 wt.% NPX compared to the high drug content sample. The higher HPMC content therefore enables easier penetration of the release medium into the filament, resulting in faster drug release.

Figure 4-23 shows the SEM images of the filaments´ cross-sections of all investigated formulations. The left column (a, c, e) shows all the formulations containing 10 wt.% NPX while the right column (b, d, f) shows the ones containing 30 wt.% NPX. Comparing low and high drug content a clear difference in pore size and number can be seen. In general, the images show varying pore sizes for all the formulations. The filament pieces with lower drug content have small and large pores, whereas the pieces with 30 wt.% NPX mainly show larger pores, which is consistent with the images taken from the surface of the filaments. The variation of pore sizes, from very large or small cavities in the remaining PLA-matrix indicates, that some pores are the consequence of insufficient mixing in the extruder, and some are the result of the phase separation during HME.

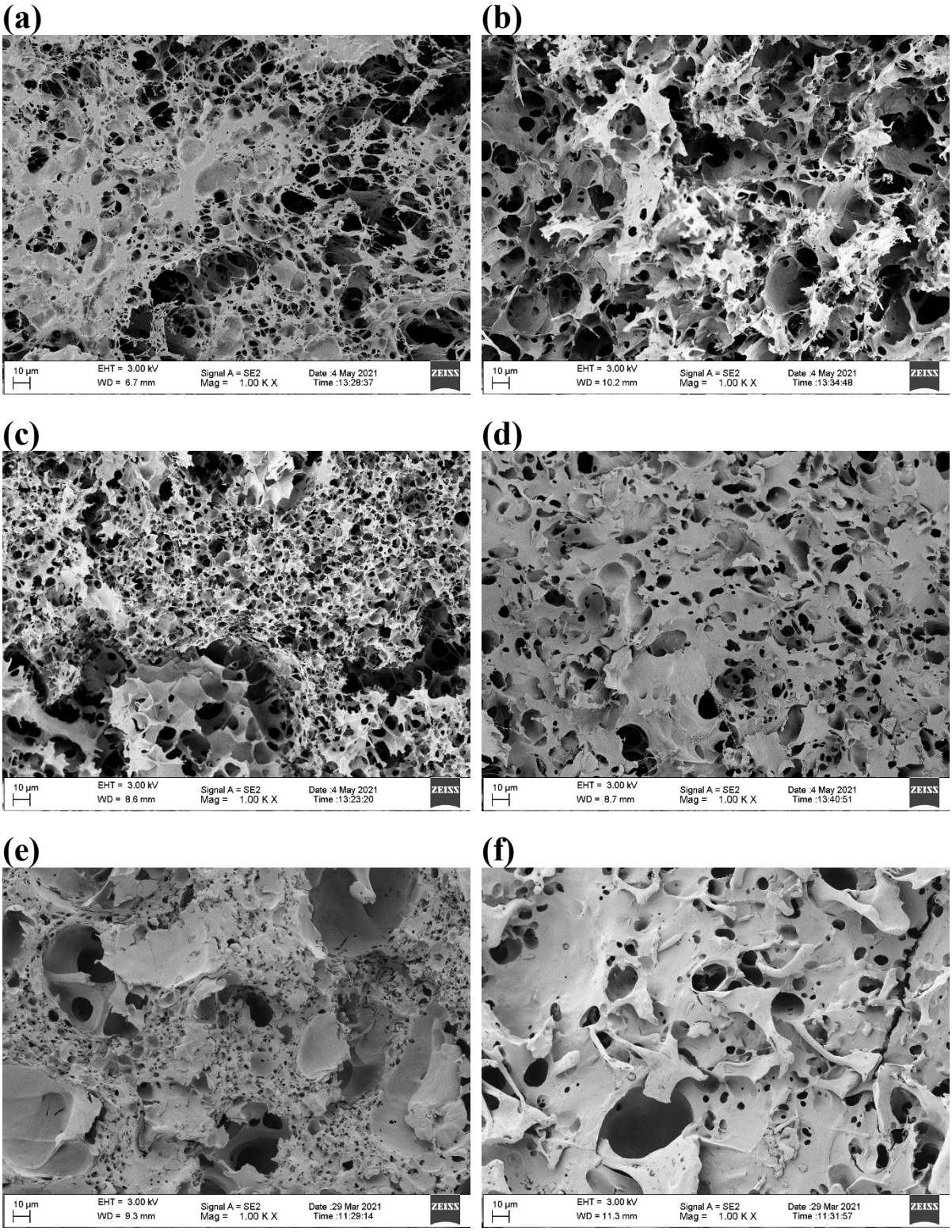

Figure 4-23: SEM-Images of filament pieces at 1k magnification after release (a) 30:70_10 wt.% NPX; (b) 30:70_30 wt.% NPX; (c) 50:50_10 wt.% NPX; (d) 50:50_30 wt.% NPX; (e) 70:30_10 wt.% NPX; (f) 70:30_30 wt.% NPX

Comparing the images for the different polymer ratios shows that an increase in PLA clearly results in a denser and less porous matrix. The samples containing 70 % PLA (e, f) are relatively dense, whereas

a far more fragile and porous matrix can be observed for the samples only containing 30 % PLA (a–d). The occurrence of larger holes means that all drug and HPMC present in this region were fully dissolved in the release medium, suggesting the formation of domains mainly containing PLA or HPMC in the filaments. For more SEM images (at 250x and 4000x magnification), cf. Appendix. These images show clear and distinct lines and boundaries for the pores and the cavities in the PLA matrix, which also suggest clear spatial boundaries of the two polymers.

5 CONCLUSION

The results obtained in this work demonstrate the possibility to use blends of already FDA approved polymers, such as HPMC and PLA to control the drug release rate. The phase separation of polymers during HME might be used. Nonetheless, sufficient knowledge about thermomechanical and flow properties is necessary to ensure a time-efficient development of the HME process. The ternary mixture of the two polymers and the model drug Naproxen exhibit significant synergistic effects, i.e. plasticization, as well as anti-plasticization, resulting in challenges to find the correct process parameter during the extrusion process. Depending on the formulation, the filaments are prone to shrink (high PLA content) or expand (high HPMC content) after extrusion. Formulations with pure PLA, or a ratio of HPMC and PLA, show no tendency of fouling during the extrusion process or degradation of the API, whereas formulations containing only HPMC and NPX exhibit defects due to fouling in the extruder.

The phase separation of the polymers during HME was characterized by thermal and spectroscopic analyses of the filaments. The blends of the two polymers show the same T_g as pure PLA in the DSC thermograms, indicating that the polymers are not fully miscible. Consequently, the T_g of the blends, with and without NPX, does not follow the Gordon-Taylor equation, reinforcing the spatial separation. Additionally, the DSC study showed that NPX has a significant plasticizing effect on PLA.

Furthermore, ATR-FTIR measurements indicate no interactions between the two polymers due to the absence of any peak shifts for the polymer mixtures. However, the spectroscopy analysis shows hydrogen bonds between PLA and NPX which may be beneficial for the solid stability of the ASD. The formation of ASDs was confirmed with WAXS for all formulations, demonstrating the possibility to enhance the solubility and bioavailability of low-water-soluble drugs with a polymer blend. With Raman mapping, it is possible to visualize the phase behaviour after extrusion and before the release studies.

Dissolution studies qualitatively confirmed these observations made by the quantitative analysis. Using a polymer blend with different ratios of the hydrophilic (HPMC) and the hydrophobic polymer (PLA), the release performance of the drug can be significantly influenced. Furthermore, the results show that pure HPMC as a polymeric carrier is not suitable due to fouling in the extruder and insufficient mechanical flexibility. Pure PLA shows almost no release over a period of four weeks and is therefore not suitable for oral administration. However, the ternary mixtures with a polymer blend and the incorporated drug exhibit stable and uniform release profiles. For formulations with HPMC as the predominate polymer, the drug release rate was significantly faster than for formulations with PLA as the predominate polymer.

The hydrophobic PLA matrix provides a template for forming water-filled pores during the dissolution of HPMC and NPX, and the pore formation controls the release rate. Furthermore, the HPMC-matrix might be able to prohibit recrystallisation of the drug during release. The PLA matrix analysed by SEM visualizes the pore formation within the matrix and shows different scales of the created polymer domains. Since the creation of domains was already confirmed before release, the possibility of a water-induced polymer phase separation was excluded.

In conclusion, the possibility of tailoring the release profile provides a valuable tool in the formulation development of personalized medicine using the same excipients in various proportions to control the drug release rates or release profiles. Except for the polymer ratio, the release profile can also be tailored by the surface area and the drug content. Therefore, the utilization of polymer blends, and the corresponding phase separation during HME, shows a novel way to create extended drug release profiles for low water-soluble drugs. Using blends of already approved polymers avoids the costly and complicated approval process of new excipients in formulation development but new structural demands and tailoring of release profiles can be achieved regardless.

Nonetheless, further investigation concerning e.g. the recrystallisation behaviour and the long-term stability of the drug inside the ASDs is needed, to ensure sufficient stability of the formulations.

6 REFERENCES

[1] R. Govender, S. Abrahmsén-Alami, A. Larsson, and S. Folestad, 'Therapy for the individual: Towards patient integration into the manufacturing and provision of pharmaceuticals', *European Journal of Pharmaceutics and Biopharmaceutics*, vol. 149. Elsevier B.V., pp. 58–76, Apr. 01, 2020, doi: 10.1016/j.ejpb.2020.01.001.

[2] X. Zhu, H. Li, L. Huang, M. Zhang, W. Fan, and L. Cui, '3D printing promotes the development of drugs', *Biomedicine and Pharmacotherapy*, vol. 131. Elsevier Masson SAS, p. 110644, Nov. 01, 2020, doi: 10.1016/j.biopha.2020.110644.

[3] G. Gorkem Buyukgoz, D. Soffer, J. Defendre, G. M. Pizzano, and R. N. Davé, 'Exploring tablet design options for tailoring drug release and dose via fused deposition modeling (FDM) 3D printing', *Int. J. Pharm.*, vol. 591, p. 119987, Dec. 2020, doi: 10.1016/j.ijpharm.2020.119987.

[4] P. Poechlauer, J. Manley, R. Broxterman, rn Gregertsen, and M. Ridemark, 'Continuous Processing in the Manufacture of Active Pharmaceutical Ingredients and Finished Dosage Forms: An Industry Perspective', 2012, doi: 10.1021/op300159y.

[5] P. Poechlauer *et al.*, 'Pharmaceutical Roundtable Study Demonstrates the Value of Continuous Manufacturing in the Design of Greener Processes', *Org. Process Res. Dev.*, vol. 17, no. 12, pp. 1472–1478, 2013, doi: 10.1021/op400245s.

[6] M. A. Repka *et al.*, 'Melt extrusion with poorly soluble drugs – An integrated review', *Int. J. Pharm.*, vol. 535, no. 1–2, pp. 68–85, Jan. 2018, doi: 10.1016/j.ijpharm.2017.10.056.

[7] M. F. Simões, R. M. A. Pinto, and S. Simões, 'Hot-melt extrusion in the pharmaceutical industry: toward filing a new drug application', *Drug Discovery Today*, vol. 24, no. 9. Elsevier Ltd, pp. 1749–1768, Sep. 01, 2019, doi: 10.1016/j.drudis.2019.05.013.

[8] T. Vasconcelos, B. Sarmento, and P. Costa, 'Solid dispersions as strategy to improve oral bioavailability of poor water soluble drugs', *Drug Discov. Today*, vol. 12, no. 23, pp. 1068–1075, 2007, doi: https://doi.org/10.1016/j.drudis.2007.09.005.

[9] A. Q. Vo, J. Zhang, D. Nyavanandi, S. Bandari, and M. A. Repka, 'Hot melt extrusion paired fused deposition modeling 3D printing to develop hydroxypropyl cellulose based floating tablets of cinnarizine', *Carbohydr. Polym.*, vol. 246, p. 116519, Oct. 2020, doi: 10.1016/j.carbpol.2020.116519.

[10] R. Govender, 'Integrated Product and Process Design for Mass Customization: A Road Towards Patient Access to Individualized Pharmaceutical Therapy', Chalmers University of Technology, 2021.

[11] N. N. Nyamweya, 'Applications of polymer blends in drug delivery', *Futur. J. Pharm. Sci.*, vol. 7, no. 1, p. 18, 2021, doi: 10.1186/s43094-020-00167-2.

[12] A. K. Bajpai, S. Shukla, S. Bhanu, and S. Kankane, 'Responsive Polymers in Controlled Drug Delivery', *Prog. Polym. Sci.*, vol. 33, pp. 1088–1118, Nov. 2008, doi: 10.1016/j.progpolymsci.2008.07.005.

[13] H. Van Ngo *et al.*, 'Hydrophilic-hydrophobic polymer blend for modulation of crystalline changes and molecular interactions in solid dispersion', *Int. J. Pharm.*, vol. 513, no. 1–2, pp. 148–152, Nov. 2016, doi: 10.1016/j.ijpharm.2016.09.017.

[14] 'Methods and Techniques for Synthesis, Characterization, Processing, and Modification of Polymers', in *Polymer Synthesis: Theory and Practice: Fundamentals, Methods, Experiments*, Berlin, Heidelberg: Springer Berlin Heidelberg, 2005, pp. 39–156.

[15] H. Andersson, 'Structure control by phase separation and influence on mass transport in films for controlled release', Chalmers University of Technology, 2015.

[16] S. Saboo, D. E. Moseson, U. S. Kestur, and L. S. Taylor, 'Patterns of drug release as a function of drug loading from amorphous solid dispersions: A comparison of five different polymers', 2020, doi: 10.1016/j.ejps.2020.105514.

[17] X. Ma and R. O. Williams, 'Characterization of amorphous solid dispersions: An update', *Journal of Drug Delivery Science and Technology*, vol. 50. Editions de Sante, pp. 113–124, Apr. 01, 2019, doi: 10.1016/j.jddst.2019.01.017.

[18] S. Baghel, H. Cathcart, and N. J. O'Reilly, 'Polymeric Amorphous Solid Dispersions: A Review of Amorphization, Crystallization, Stabilization, Solid-State Characterization, and Aqueous Solubilization of Biopharmaceutical Classification System Class II Drugs', *Journal of Pharmaceutical Sciences*, vol. 105, no. 9. Elsevier B.V., pp. 2527–2544, Sep. 01, 2016, doi: 10.1016/j.xphs.2015.10.008.

[19] R. Govender, S. Abrahmsén-Alami, A. Larsson, A. Borde, A. Liljeblad, and S. Folestad, 'Independent tailoring of dose and drug release via a modularized product design concept for mass customization', *Pharmaceutics*, vol. 12, no. 8, pp. 1–24, 2020, doi: 10.3390/pharmaceutics12080771.

[20] J. Zhang *et al.*, 'Development and evaluation of pharmaceutical 3D printability for hot melt extruded cellulose-based filaments', *J. Drug Deliv. Sci. Technol.*, vol. 52, pp. 292–302, Aug. 2019, doi: 10.1016/j.jddst.2019.04.043.

[21] W.-K. Hsiao, B. Lorber, H. Reitsamer, and J. Khinast, 'Expert Opinion on Drug Delivery 3D printing of oral drugs: a new reality or hype?', 2017, doi: 10.1080/17425247.2017.1371698.

[22] J. Zhang *et al.*, 'Hydroxypropyl methylcellulose-based controlled release dosage by melt extrusion and 3D printing: Structure and drug release correlation', *Carbohydr. Polym.*, vol. 177, pp. 49–57, Dec. 2017, doi: 10.1016/j.carbpol.2017.08.058.

[23] M. Maniruzzaman *et al.*, 'A Review of Hot-Melt Extrusion: Process Technology to Pharmaceutical Products', *Int. Sch. Res. Netw. ISRN Pharm.*, vol. 2012, 2012, doi: 10.5402/2012/436763.

[24] A. L. Sarode, H. Sandhu, N. Shah, W. Malick, and H. Zia, 'Hot melt extrusion (HME) for amorphous solid dispersions: Predictive tools for processing and impact of drug-polymer interactions on supersaturation', *Eur. J. Pharm. Sci.*, vol. 48, no. 3, pp. 371–384, Feb. 2013, doi: 10.1016/j.ejps.2012.12.012.

[25] B. Démuth *et al.*, 'Downstream processing of polymer-based amorphous solid dispersions to generate tablet formulations', *International Journal of Pharmaceutics*, vol. 486, no. 1–2. Elsevier, pp. 268–286, May 30, 2015, doi: 10.1016/j.ijpharm.2015.03.053.

[26] S. Mascia *et al.*, 'End-to-end continuous manufacturing of pharmaceuticals: Integrated synthesis, purification, and final dosage formation', *Angew. Chemie - Int. Ed.*, vol. 52, no. 47, pp. 12359–12363, Nov. 2013, doi: 10.1002/anie.201305429.

[27] G. M. Keserü and G. M. Makara, 'The influence of lead discovery strategies on the properties of drug candidates', *Nat. Rev. Drug Discov.*, vol. 8, no. 3, pp. 203–212, 2009, doi: 10.1038/nrd2796.

[28] L. M. Mayr and D. Bojanic, 'Novel trends in high-throughput screening', *Current Opinion in Pharmacology*, vol. 9, no. 5. Elsevier, pp. 580–588, Oct. 01, 2009, doi: 10.1016/j.coph.2009.08.004.

[29] T. Vasconcelos, S. Marques, J. das Neves, and B. Sarmento, 'Amorphous solid dispersions: Rational selection of a manufacturing process', *Advanced Drug Delivery Reviews*, vol. 100. Elsevier B.V., pp. 85–101, May 01, 2016, doi: 10.1016/j.addr.2016.01.012.

[30] M. S. Ku, 'Use of the biopharmaceutical classification system in early drug development', *AAPS J.*, vol. 10, no. 1, pp. 208–212, 2008, doi: 10.1208/s12248-008-9020-0.

[31] A. Q. Vo, J. Zhang, D. Nyavanandi, S. Bandari, and M. A. Repka, 'Hot melt extrusion paired fused deposition modeling 3D printing to develop hydroxypropyl cellulose based floating tablets of cinnarizine', *Carbohydr. Polym.*, vol. 246, p. 116519, 2020, doi: 10.1016/j.carbpol.2020.116519.

[32] I. M. Kalogeras and W. Brostow, 'Glass Transition Temperatures in Binary Polymer Blends', *J. Polym. Sci. Part B Polym. Phys.*, vol. 47, pp. 80–95, 2009, doi: 10.1002/polb.21616.

[33] M. Gordon and J. S. Taylor, 'Ideal copolymers and the second-order transitions of synthetic rubbers. i. non-crystalline copolymers', *J. Appl. Chem.*, vol. 2, no. 9, pp. 493–500, 1952, doi: https://doi.org/10.1002/jctb.5010020901.

[34] Nutrition and Bioscience DuPont, 'Affinisol ™ Hpmc Hme', [Online]. Available: https://www.pharma.dupont.com/content/dam/dupont/amer/us/en/nutrition-health/general/pharmaceuticals/documents/Download_Affinisol HPMC HME Brochure.pdf.

[35] B. Tyler, D. Gullotti, A. Mangraviti, T. Utsuki, and H. Brem, 'Polylactic acid (PLA) controlled delivery carriers for biomedical applications ☆', 2016, doi: 10.1016/j.addr.2016.06.018.

[36] S. Farah, D. G. Anderson, and R. Langer, 'Physical and mechanical properties of PLA, and their functions in widespread applications — A comprehensive review', *Advanced Drug Delivery Reviews*, vol. 107. Elsevier B.V., pp. 367–392, Dec. 15, 2016, doi: 10.1016/j.addr.2016.06.012.

[37] Y. Huang and W.-G. Dai, 'Fundamental aspects of solid dispersion technology for poorly soluble drugs', *Acta Pharm. Sin. B*, vol. 4, no. 1, pp. 18–25, Feb. 2014, doi: 10.1016/j.apsb.2013.11.001.

[38] M. Parolini, 'Toxicity of the Non-Steroidal Anti-Inflammatory Drugs (NSAIDs) acetylsalicylic acid, paracetamol, diclofenac, ibuprofen and naproxen towards freshwater invertebrates: A review', *Science of the Total Environment*, vol. 740. Elsevier B.V., p. 140043, Oct. 20, 2020, doi: 10.1016/j.scitotenv.2020.140043.

[39] M. Mokhtarpour, H. Shekaari, F. Martinez, and M. T. Zafarani-Moattar, 'Study of naproxen in some aqueous solutions of choline-based deep eutectic solvents: Solubility measurements, volumetric and compressibility properties', *Int. J. Pharm.*, vol. 564, pp. 197–206, Jun. 2019, doi: 10.1016/j.ijpharm.2019.04.029.

[40] S. Abbott, 'Solubility, similarity, and compatibility: A general-purpose theory for the formulator', *Current Opinion in Colloid and Interface Science*, vol. 48. Elsevier Ltd, pp. 65–76, Aug. 01, 2020, doi: 10.1016/j.cocis.2020.03.007.

[41] C. Hansen, *Hansen Solubility Parameters: A User's Handbook, Second Edition*. 2012.

[42] S. Abbott, 'Chemical Compatibility of Poly(Lactic Acid): A Practical Framework Using Hansen Solubility Parameters', *Poly(Lactic Acid) Synth. Struct. Prop. Process. Appl.*, pp. 83–95, 2010, doi: 10.1002/9780470649848.ch7.

[43] M. G. Davanço, D. R. Campos, and P. de O. Carvalho, 'In vitro – In vivo correlation in the development of oral drug formulation: A screenshot of the last two decades', *International Journal of Pharmaceutics*, vol. 580. Elsevier B.V., p. 119210, Apr. 30, 2020, doi: 10.1016/j.ijpharm.2020.119210.

[44] S. Saboo, N. A. Mugheirbi, D. Y. Zemlyanov, U. S. Kestur, and L. S. Taylor, 'Congruent release of drug and polymer: A "sweet spot" in the dissolution of amorphous solid dispersions', *J. Control. Release*, vol. 298, pp. 68–82, Mar. 2019, doi: 10.1016/j.jconrel.2019.01.039.

[45] M. S. Paolini, O. S. Fenton, C. Bhattacharya, J. L. Andresen, and R. Langer, 'Polymers for extended-release administration', *Biomed. Microdevices*, vol. 21, no. 2, p. 45, 2019, doi: 10.1007/s10544-019-0386-9.

[46] C. Dempster, 'Coupling of Hot-melt Extrusion and 3-Dimensional Printing in the Production of Insoluble Matrices for Controlled Drug Deliveryitle', Chalmers University of Technology, 2020.

[47] J. Currie, 'Development and Characterisation of Hot-Melt Extruded Water Soluble Extended Release Dosage Formulations for Use in Fused Deposition Modelling', Chalmers University of Technology, 2020.

[48] T. Heikkilä *et al.*, 'Equilibrium drug solubility measurements in 96-well plates reveal similar drug solubilities in phosphate buffer pH 6.8 and human intestinal fluid', *Int. J. Pharm.*, vol. 405, no. 1–2, pp. 132–136, Feb. 2011, doi: 10.1016/j.ijpharm.2010.12.007.

[49] 'Partial-solubility Parameters of Naproxen and Sodium Diclofenac', 1998. doi: 10.1111/j.2042-7158.1998.tb06911.x.

[50] D. Garlotta, 'A Literature Review of Poly(Lactic Acid)', *J. Polym. Environ.*, vol. 9, no. 2, pp. 63–84, 2001, doi: 10.1023/A:1020200822435.

[51] A. Paudel, J. Van Humbeeck, and G. Van Den Mooter, 'Theoretical and experimental investigation on the solid solubility and miscibility of naproxen in poly(vinylpyrrolidone)', *Mol. Pharm.*, vol. 7, no. 4, pp. 1133–1148, Aug. 2010, doi: 10.1021/mp100013p.

[52] A. Paudel, E. Nies, and G. Van den Mooter, 'Relating Hydrogen-Bonding Interactions with the Phase Behavior of Naproxen/PVP K 25 Solid Dispersions: Evaluation of Solution-Cast and Quench-Cooled Films', *Mol. Pharm.*, vol. 9, no. 11, pp. 3301–3317, Nov. 2012, doi: 10.1021/mp3003495.

[53] M. Wrona, M. J. Cran, C. Nerín, and S. W. Bigger, 'Development and characterisation of HPMC films containing PLA nanoparticles loaded with green tea extract for food packaging applications', *Carbohydr. Polym.*, vol. 156, pp. 108–117, Jan. 2017, doi: 10.1016/j.carbpol.2016.08.094.

[54] L. Kumar, B. S. Suhas, K. Girish Pai, and R. Verma, 'Determination of saturated solubility of naproxen using UV visible spectrophotometer', *Res. J. Pharm. Technol.*, vol. 8, no. 7, pp. 825–828, 2015, doi: 10.5958/0974-360X.2015.00134.1.

[55] M. Marucci, J. Hjärtstam, G. Ragnarsson, F. Iselau, and A. Axelsson, 'Coated formulations: New insights into the release mechanism and changes in the film properties with a novel release cell', *J. Control. Release*, vol. 136, no. 3, pp. 206–212, Jun. 2009, doi: 10.1016/j.jconrel.2009.02.017.

[56] P. L. Ritger and N. A. Peppas, 'A simple equation for description of solute release II. Fickian and anomalous release from swellable devices', *J. Control. Release*, vol. 5, no. 1, pp. 37–42, 1987, doi: 10.1016/0168-3659(87)90035-6.

[57] P. L. Ritger and N. A. Peppas, 'A simple equation for description of solute release I. Fickian and non-fickian release from non-swellable devices in the form of slabs, spheres, cylinders or discs', *J. Control. Release*, vol. 5, no. 1, pp. 23–36, Jun. 1987, doi: 10.1016/0168-3659(87)90034-4.

7 APPENDIX

7.1 CALIBRATION CURVE

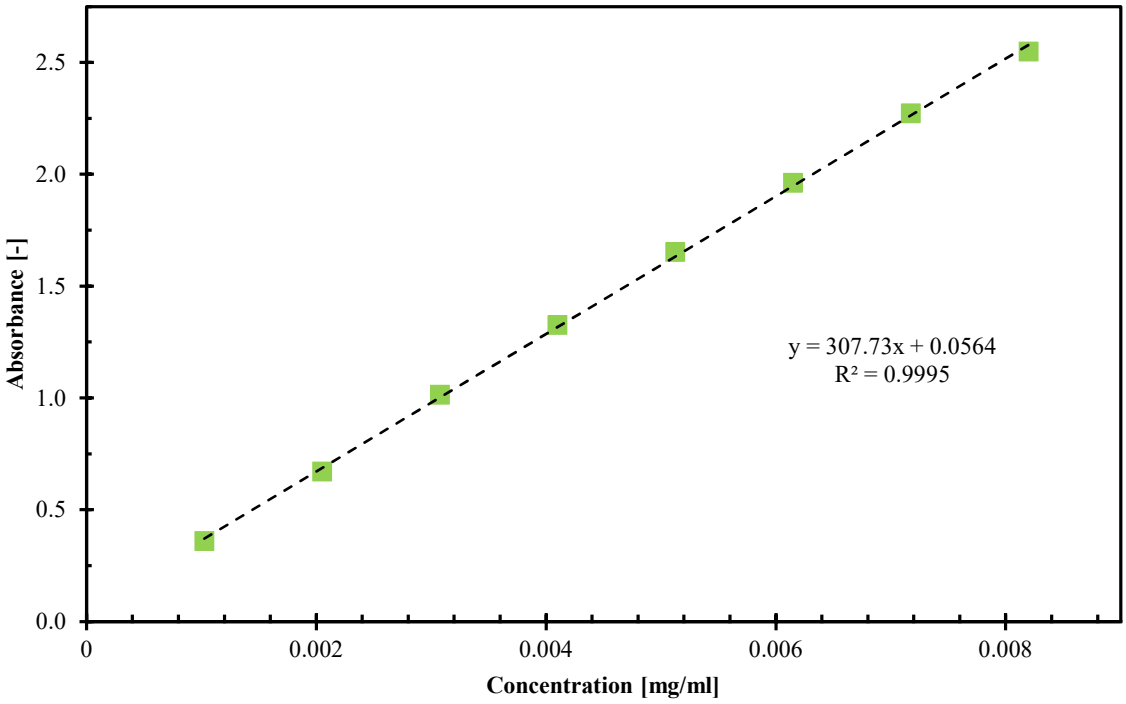

Figure 7-1: Calibration curve of Naproxen for the UV-Vis analysis

7.2 ATR-FTIR RAW DATA

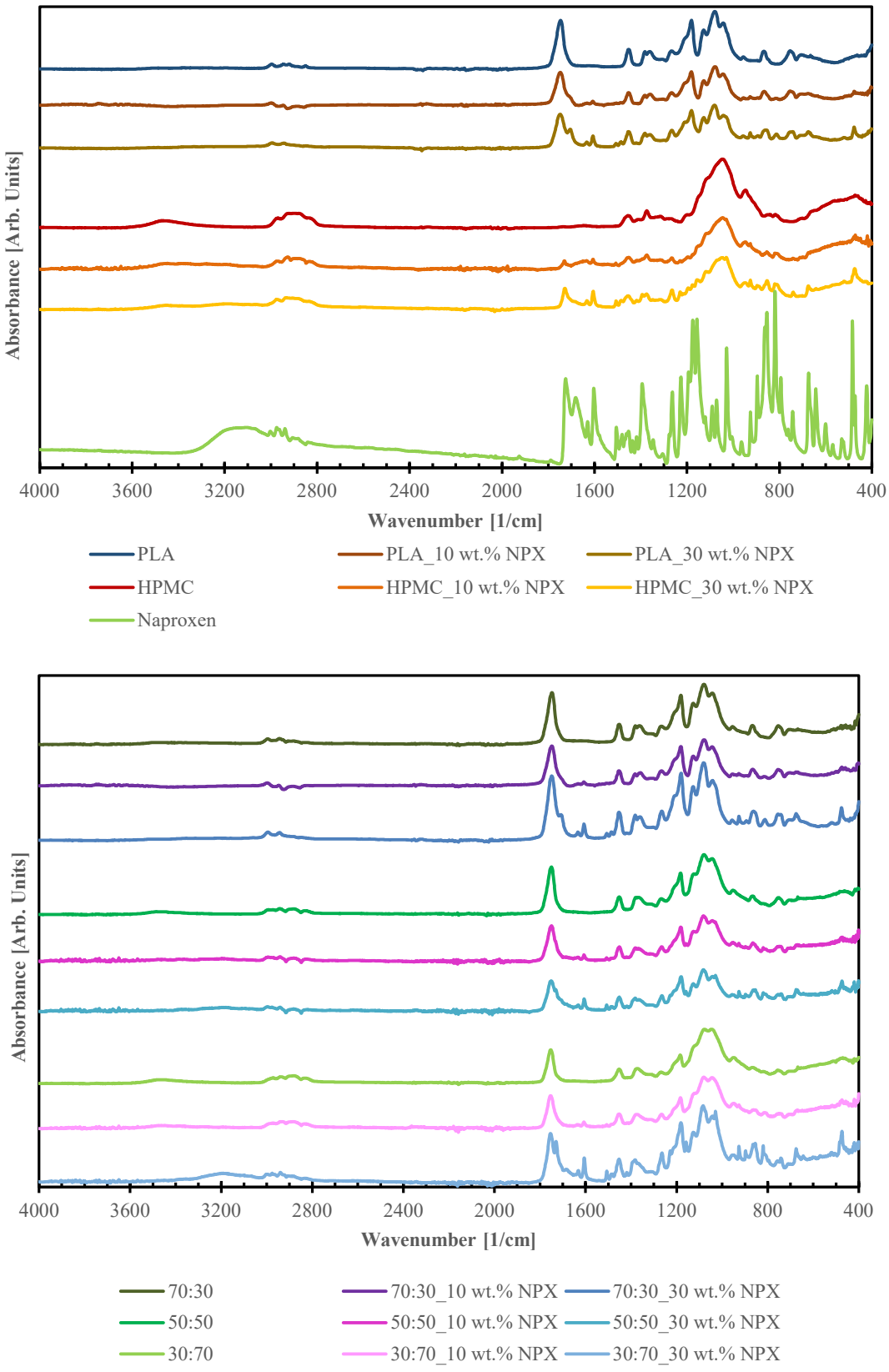

Figure 7-2: Complete ATR-FTIR spectra of the investigated formulations

7.3 ADDITIONAL SEM IMAGES

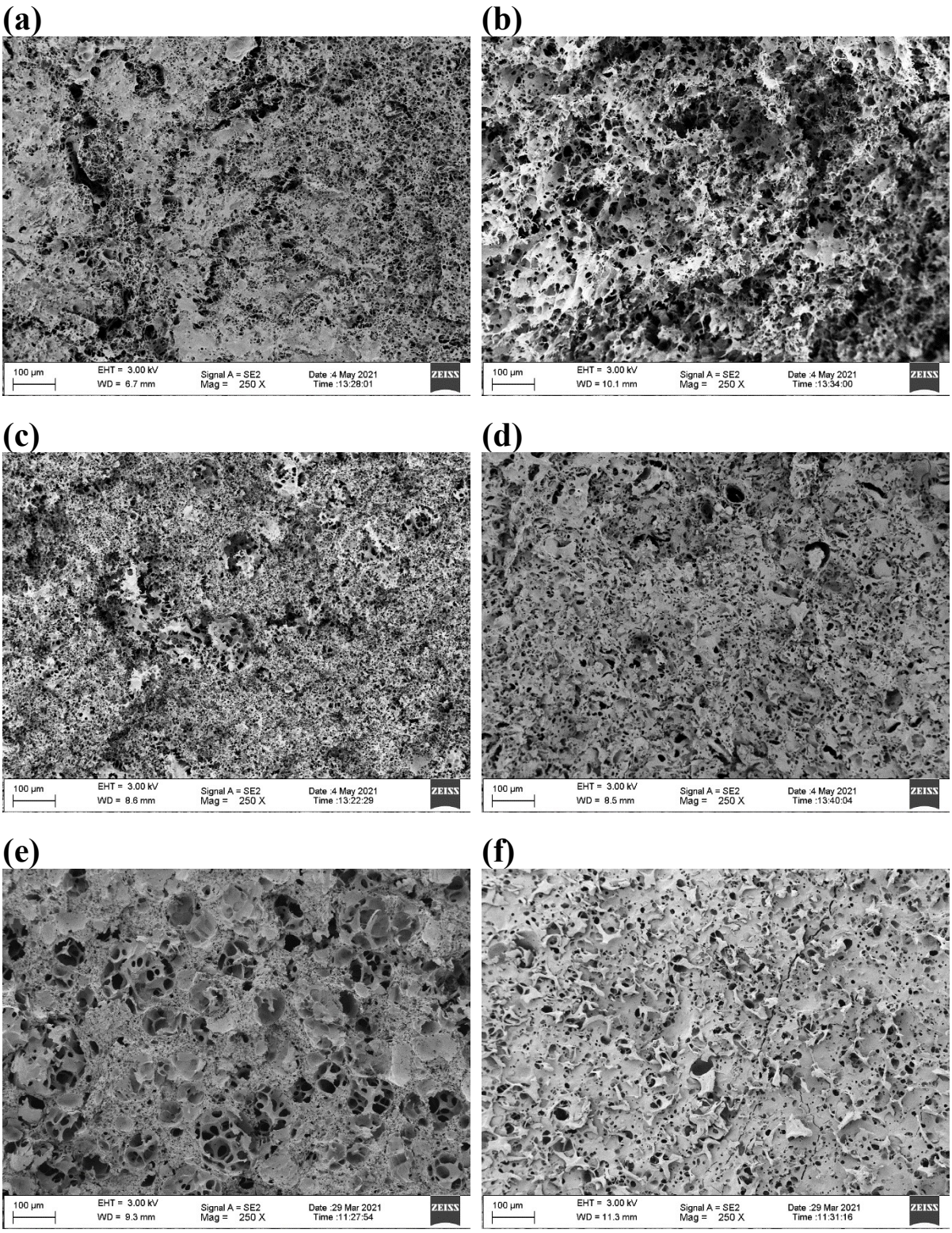

Figure 7-3: SEM-Images of filament pieces at 250x magnification after release (a) 30:70_10wt.%NPX; (b) 30:70_30wt.%NPX; (c) 50:50_10wt.%NPX; (d) 50:50_30wt.%NPX; (e) 70:30_10wt.%NPX; (f) 70:30_30wt.%NPX

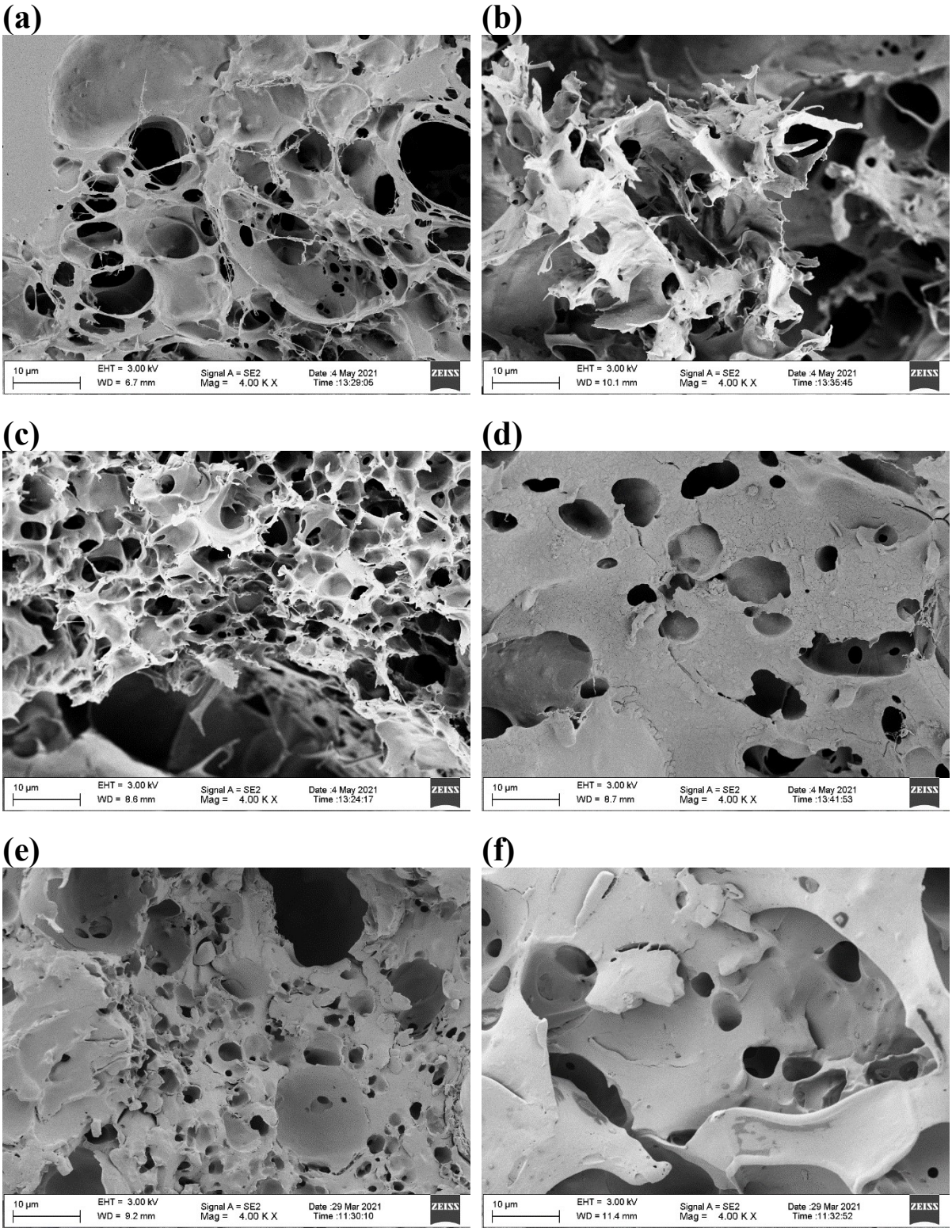

Figure 7-4: SEM-Images of filament pieces at 4k magnification after release (a) 30:70_10wt.%NPX; (b) 30:70_30wt.%NPX; (c) 50:50_10wt.%NPX; (d) 50:50_30wt.%NPX; (e) 70:30_10wt.%NPX; (f) 70:30_30wt.%NPX

7.4 LIST OF FIGURES

7.5 LIST OF TABLES